Schweizerische Eidgenossenschaft
Confédération suisse
Confederazione Svizzera
Confederaziun svizra

Federal Department of the Environment, Transport, Energy and Communications DETEC

Swiss Federal Office of Energy SFOE
Energy Research and Cleantech Division

Final report dated 30.08.2021

Wandintegrierte innovative Prallkühlungsgeometrien für fortschrittliche Turbinenschaufeln

Date: 30.08.2021

Location: Lausanne/Baden

Publisher:
Swiss Federal Office of Energy SFOE
Energy Research and Cleantech
CH-3003 Bern
www.bfe.admin.ch

Subsidy recipients:
EPFL - Swiss Federal Institute of Technology
Group of Thermal Turbomachinery (GTT)
Station 9
CH-1015 Lausanne
https://gtt.epfl.ch/

ANSALDO Energia Switzerland
Römerstrasse 36
CH-5401 Baden
http://www.ansaldoenergia.com

Authors:
Michele Gaffuri, EPFL-GTT, michele.gaffuri@epfl.ch
Naik Shailendra, Ansaldo Energia Switzerland, Shailendra.Naik@ansaldoenergia.com

SFOE project coordinators:
Peter Jansohn, Paul Scherrer Institut, peter.jansohn@psi.ch
Men.Wirz@bfe.admin.ch

SFOE contract number: SI/501505-01

The authors bear the entire responsibility for the content of this report and for the conclusions drawn therefrom.

Zusammenfassung

Die Stromerzeugung mit Gasturbinen ist ein wichtiges Instrument für die Dekarbonisierung der Stromerzeugung, da sie eine schnell disponierbare Stromquelle ist, die zur Stabilisierung des Stromnetzes genutzt werden kann, wenn die Nachfrage die Produktion übersteigt. Durch die Verbrennung von synthetischem Gas oder Wasserstoff, der mit überschüssiger erneuerbarer Energie in Zeiten geringer Nachfrage erzeugt wird, fungieren Gasturbinenanlagen als ein Teil eines Energiespeichersystems. Um den Wirkungsgrad des Gasturbinenkreislaufs zu erhöhen, muss die Verbrennungstemperatur erhöht werden; deswegen, müssen die Turbinenteile aktiv gekühlt werden, um der heißen Gastemperatur standzuhalten. Da die Kühlluft aus dem Verdichter entnommen wird, verbessert eine Reduzierung der zur Kühlung verwendeten Luftmenge auch den Wirkungsgrad der Maschine.

In diesem Projekt wurden sequenzielle Impingement-Kühlkanäle experimentell evaluiert. Die sequenzielle Prallkühlung ist ein neuartiges Konzept der Turbinenschaufelkühlung, bei dem die Kühlluft zweimal zur Prallkühlung verwendet wird, bevor sie zur Filmkühlung eingesetzt wird. Ziel ist es, das Kühlpotenzial des Fluids besser auszunutzen und so die Menge des verwendeten Kühlmittels zu reduzieren oder die Verbrennungstemperatur zu erhöhen (oder eine Kombination von beidem).

Mehr als 30 verschiedene Kühlkanalkonfigurationen wurden experimentell untersucht, um die besten Lösungen in Bezug auf die Wärmeübertragungseigenschaften der Strömung und die Druckverluste durch den Kanal zu ermitteln. Die Tests werden an skalierten Geometrien unter Anwendung einer Variation der transienten Flüssigkristallthermografie-Methode durchgeführt, um mit hoher räumlicher Auflösung den Wärmeübergangskoeffizienten auf der Zieloberfläche zu bestimmen. Die Druckwerte an verschiedenen Stellen entlang des Kanals wurden gemessen, um Informationen über die Druckverluste der gesamten Kühlgeometrie zu sammeln und zu ermitteln, welcher Teil des Kanals am meisten zu den Verlusten beiträgt.

Die leistungsstärksten Konfigurationen wurden dann in einen analytischen Rahmen integriert, um die potenzielle Verbesserung in Bezug auf den Kraftstoffverbrauch der neuartigen Kühllösungen zu bewerten. Dabei wird eine Gasturbine auf dem aktuellen Stand der Technik betrachtet und die Auswirkung der Reduzierung des Kühlmittelmassenstroms bewertet. Die Lösung mit der besten Wärmeübertragung ermöglicht eine Erhöhung des thermischen Wirkungsgrads der Turbine von 42.18 % auf 42.65 %. Dies entspricht einer Reduzierung des Brennstoffverbrauchs bei gleicher erzeugter Leistung um 1.11 %. Im globalen Maßstab würde diese Verbesserung die CO2-Emissionen der gasbefeuerten Anlagen um etwa 20000 Tonnen pro Jahr reduzieren. Darüber hinaus könnten ähnliche Kühlkonfigurationen im Bereich der Flugzeugantriebe mit ähnlichen Effizienzverbesserungen und CO_2-Einsparungen implementiert werden.

Résumé

La production d'électricité par turbine à gaz est un outil important pour la décarbonisation de la production d'électricité, car il s'agit d'une source d'électricité rapidement mobilisable, qui peut être utilisée pour stabiliser le réseau électrique lorsque la demande dépasse la production. En brûlant du gaz synthétique ou de l'hydrogène, produit à partir de l'énergie renouvelable excédentaire en période de faible demande, les centrales à turbine à gaz font partie d'un système de stockage de l'énergie. Pour augmenter l'efficacité du cycle de la turbine à gaz, la température de combustion doit être augmentée ; les pièces de la turbine doivent être activement refroidies afin de résister à la température élevée du gaz. Comme l'air de refroidissement est extrait du compresseur, la réduction de la quantité d'air utilisée pour le refroidissement améliore également l'efficacité de la machine.

Dans ce projet, l'objectif est d'évaluer expérimentalement les canaux séquentiels de refroidissement par jets. Le refroidissement séquentiel par jet est un nouveau concept de refroidissement des aubes de turbine, dans lequel l'air de refroidissement est utilisé deux fois pour le refroidissement par jets

avant d'être utilisé pour le refroidissement par film. L'objectif est de mieux utiliser le potentiel de refroidissement du fluide, et donc de réduire la quantité de liquide de refroidissement utilisée, ou d'augmenter la température de combustion (ou une combinaison des deux).

Plus de 30 différentes configurations de canaux de refroidissement ont été évaluées expérimentalement pour identifier les meilleures solutions en termes de caractéristiques de transfert de chaleur et de pertes de pression à travers le canal. Des tests sont effectués sur des géométries à échelle agrandie en utilisant une variation de la méthode de thermographie transitoire à cristaux liquides pour déterminer avec une haute résolution spatiale le coefficient de transfert de chaleur sur la surface cible, tandis que les niveaux de pression sont mesurés en différents points du canal pour recueillir des informations sur les pertes de pression de la géométrie de refroidissement complète et identifier les parties du canal qui contribuent le plus aux pertes.

Les configurations les plus performantes sont ensuite intégrées dans un cadre analytique pour évaluer l'amélioration potentielle en termes de consommation de carburant d'une machine intégrant ces nouvelles solutions de refroidissement. Pour cela, une turbine à gaz de pointe est considérée, et l'effet de la réduction du débit massique du liquide de refroidissement est évalué. La solution la plus performante en termes de transfert de chaleur permet d'augmenter l'efficacité thermique de la turbine de 42.18% à 42.65% ; cela représente une réduction de la consommation de carburant de 1.11%, pour la même puissance de génération. À l'échelle mondiale, cette amélioration permettrait de réduire les émissions de CO2 des centrales à gaz d'environ 20 000 tonnes par an. En outre, des solutions similaires pourraient être mises en œuvre dans le domaine des systèmes de propulsion des avions, avec des améliorations d'efficacité similaires.

Summary

Gas turbine power generation is an important tool for the decarbonisation of the electricity production, since it is a fast dispatchable source of electricity that can be used to stabilise the electrical grid when demand exceeds production. By burning synthetic gas or hydrogen, produced using excess renewable energy in times of low demand, gas turbine plants act as one part of an energy storage system. To increase the efficiency of the gas turbine cycle, the combustion temperature needs to be increased; the turbine parts need to be actively cooled in order to withstand the hot gas temperature. Since the cooling air is extracted from the compressor, reducing the amount of air used for cooling also improves the efficiency of the machine.

In this project, the aim is to evaluate experimentally sequential impingement cooling channels. Sequential impingement cooling is a novel concept of turbine blades cooling, in which the cooling air is used two times for impingement cooling before being used for film cooling. The purpose of this is to make a better use of the cooling potential of the fluid, and thus reduce the amount of coolant used, or increase the combustion temperature (or a combination of both).

More than 30 different cooling channel configurations have been experimentally evaluated to identify the best solutions in terms of heat transfer characteristics of the flow and pressure losses through the channel. Tests are carried out on scaled-up geometries using a variation of the transient liquid crystal thermography method to determine with high spatial resolution the heat transfer coefficient on the target surface, while pressure levels are measured at different points along the channel to collect information on the pressure losses of the complete cooling geometry and identify which part of the channel contributes most to the losses.

The best-performing configurations are then integrated in an analytical framework to assess the potential improvement in terms of fuel consumption of the machine using the novel cooling solutions. For this, a state-of-the-art gas turbine is considered, and the effect of the reduction of the coolant massflow is evaluated. The best performing solution in terms of heat transfer allows to increase the thermal efficiency of the turbine from 42.18% to 42.65%; this represents a reduction in fuel

consumption of 1.11%, for the same generating power. On a global scale, this improvement would reduce the CO_2 emissions of the gas fired plants by approximately 20000 tons per year. Moreover, similar solutions could be implemented in the field of aircraft propulsion systems, with similar efficiency improvements.

Main findings

- The project analysed novel cooling configurations for the hot parts of a gas turbine using a novel experimental technique.
- Better performing cooling configurations allow to increase the thermal efficiency of gas turbines via an increase of the turbine entry temperature or a reduction of the cooling fluid used.
- The best performing cooling configurations analysed would allow to reduce the fuel consumption of a gas turbine by more than 2%. Worldwide, such an improvement would reduce the emissions of gas fired power plants by more than 50000 tons of CO_2.
- It is foreseen to use gas turbines as a part of an energy storage system wherein synthetic gas or hydrogen are produced using excess renewable energy (e.g. on a sunny day when production exceeds demand) and gas turbines generate electricity when the demand is high. Thermal efficiency improvements are important for achieving this vision.

Contents

Abbreviations

CMOS: Complementary metal–oxide–semiconductor

EBM: Electron beam melting

LFE: Laminar flow element

OEM: Original Equipment Manufacturers

P2G: Power to Gas

PDQ: Product Development Quality

PMMA: Poly(Methyl Methacrylate)

SHS: Stator heat shield

SLM: Synthetic laser melting

TET: Turbine entry temperature

TLC: Thermochromic liquid crystals

TRL: Technology readiness level

1 Introduction

1.1 Background information and current situation

The recently approved “Energy strategy 2050” of the Swiss Confederation calls for the reduction of the net greenhouse gas emissions to zero by 2050 in Switzerland. At the same time, the Swiss Confederation decided to phase out the existing nuclear power plants. The implementation of this strategy will result in an increase of the share of solar and wind in the energy mix. These energy sources being intermittent, strategies will have to be put in place to store this energy in times of excessive generation, to be later used when energy demand exceeds generation capacity. Although for short term storage (i.e. timeframe of less than one day) battery storage can be a potential solution, the question remains open for long term, seasonal balancing (timeframe several months).

Pumped storage power stations are operational in Switzerland and could be expanded, but will probably not meet the capacity requirements caused by the forecasted increase of electricity consumption due to the electrification of the mobility sector. In this perspective, a different storage method is needed. Power-to-gas (P2G) consists in the use of (excess) electrical power to produce fuel, usually hydrogen gas via electrolysis, which can be further processed to produce synthetic gas (methane, propane, butane). These gases can then be used in a gas turbine to convert the energy back into electricity.

Recently, ANSALDO Energia tested the possibility of using H_2 as fuel in a state-of-the-art gas turbine, showing that not only a mixture of H_2 and natural gas can be used, but also that H_2 alone can be used as fuel while complying with emission requirements in terms of NO_x [4]. This opens the possibility of using P2G as a flexible and efficient method of energy storage.

Continued progress in the efficiency of gas turbines is needed for the commercial viability of P2G plants. This depends heavily on the thermal efficiency of the gas turbine, which can be increased by increasing the maximum temperature downstream of the combustion chamber, at the inlet of the turbine stage (turbine entry temperature, TET). Since the temperature achieved exceeds the maximum admissible temperature of the material of the turbine blades and of the casing of the machine, these parts are actively cooled with compressed air bypassed from the compressor. Thus, the increase of the turbine efficiency relies on the improvement of the performances of the cooling system. Additionally, a more effective cooling system allows for the reduction of the cooling fluid massflow, which is generally bypassed from the compressor exit. Reducing this flow also has an effect on the thermal efficiency of the machine, since a higher massflow can pass through the combustion chamber and generate work in the turbine.

State of the art gas turbines can achieve a thermal efficiency – that is, the ratio of the electrical power generated to the energy content of the fuel used per unit time – above 60% when the gas turbine is coupled with a steam turbine that recovers the waste heat of the exhaust of the gas turbine (co-generation). Even a minor improvement of this value has a dramatic impact on the reduction of CO_2 emissions of gas fired plants globally.

1.2 Purpose of the project

The aim of the present project is to study and evaluate experimentally a novel solution for the cooling of turbine blades and of the casing of a gas turbine. Thanks to modern manufacturing techniques, in particular additive processes like selective laser melting (SLM) and electron beam melting (EBM), advanced cooling channels can be integrated into the components, and this allows more freedom in the design of the internal cooling passages compared to what is possible when one is constrained by the manufacturability of the piece via advanced casting.

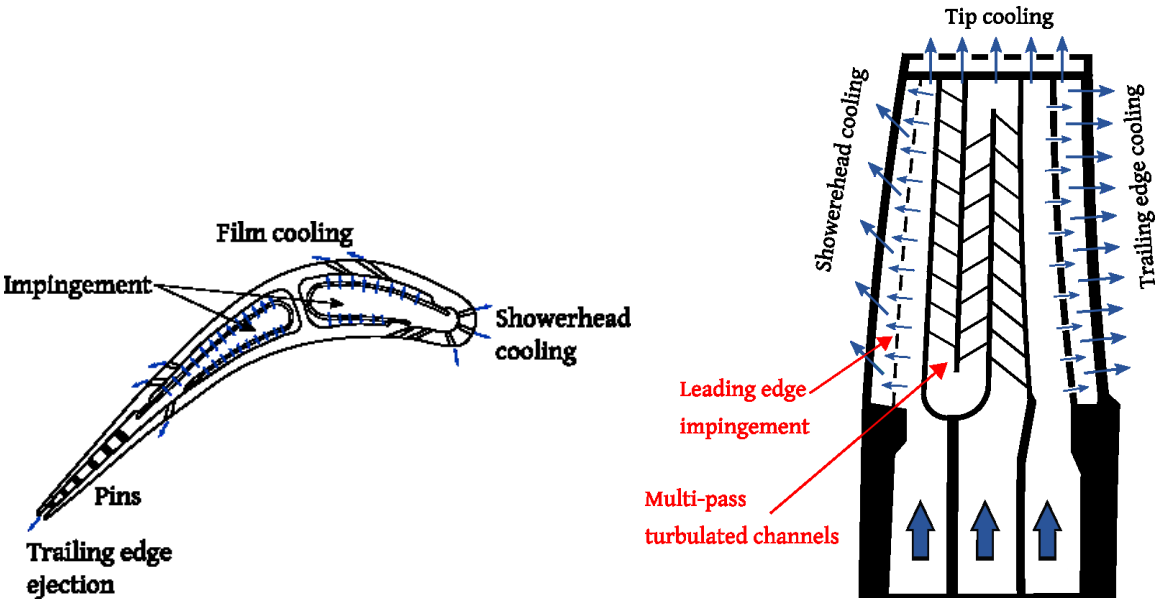

Figure 1: *Common cooling arrangements for a high pressure stator vane (left) and rotor blade (right). Drawings according to [1] and [2].*

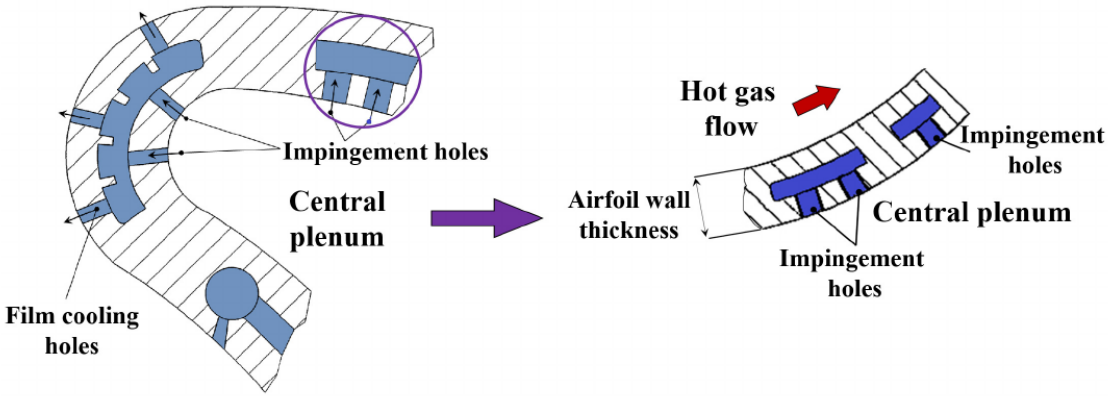

Figure 2: State-of-the-art wall-integrated impingement cooling channels. Adopted from [3].

In gas turbines, jet impingement is used on the most thermally stressed parts of the blades as it can achieve very high local heat transfer coefficients. Jet impingement has been used for many years in stator blades by inserting a perforated plate in the plenums (see Figure 1, left). This approach is not used for rotor blades due to the high centrifugal (and Coriolis) forces that modify the jet flows and create vibrations in the sheet metal insert. Instead, the rotor blade is usually only cooled by impingement at the leading edge, where the thermal loads are highest (Figure 1, right).

Recently, better performing impingement configurations have been designed and manufactured thanks to state-of-the-art investment casting techniques. In particular, so-called double-wall cooling configurations can now be implemented (see Figure 2), in which the cooling channel is integrated into the blade wall. The thinner external wall drastically increases the heat transfer. In these configurations, the impingement channel is generally arranged in a spanwise direction, with one or two rows of jets; in such a narrow channel, the heat transfer can be further enhanced by the presence of the sidewalls of the channel, which increases the area available for heat transfer.

The spent air of the jets travels along the channel and is generally ejected in the hot flow to provide a film of “cold” air protecting the external surface of the blade from the hot gas. By moving along the cooling channel, this spent air disturbs the jet flow of the downstream jets, reducing their heat transfer levels and posing a limit on the number of jets that can be placed in any single channel.

In the frame of the present project, a different approach is investigated: two shorter channels are connected in series, so that the spent air from the first channel can be reused a second time in the second channel. This potentially provides several advantages:

- the amount of cooling air is reduced: by using the same cooling air two times, the total amount of cooling fluid is reduced. Since the cooling air is bypassed from the compressor exit, this increases the efficiency of the gas turbine, since the massflow performing the whole thermodynamic cycle is increased;
- the so called crossflow effect, the interaction between the spent air and the downstream jets is reduced.

Some critical points of this cooling solution have to be addressed and analyzed:

- the more complex channel leads to increased pressure losses along the channel;
- the exit region of the first channel, the so called transition zone, cannot be cooled by impingement and could experience higher temperatures.
- The cooling air in the 2nd channel has a higher temperature and thus less cooling capacity.

The project aims to evaluate experimentally this type of channels and provide information on the suitability of their implementation in future gas turbines for impingement cooling. In order to do this, detailed maps of the heat transfer coefficients on the target surface have to be measured, as well as the pressure losses along the channel. This data will then be used to evaluate the cooling solutions proposed and estimate the potential gains in terms of efficiency of the complete gas turbine, in order to conclude on the viability of the approach.

The project builds on equipment developed for a previous project (*“Wandintegrierte Kühlungssysteme: Prallkühlung kombiniert mit komplexen Geometrien”*, contract number SI/500356-01) in which an extensive database of impingement cooling geometries has been created. Modifications of the experimental setup are required to cope with the more complex geometries to be investigated in this project.

In addition, the industrial partner integrates the knowledge gained in the lab to test the cooling solution in a test engine in real-life conditions of pressure and temperature to validate the parts and bring them to a technology readiness level (TRL) of 5.

1.3 Objectives

The principal objective of the project is the experimental evaluation of sequential impingement channels. For this, maps of the heat transfer coefficient need to be obtained on the target surface. Additionally, pressure data must be obtained in order to evaluate the suitability of the integration of such channels in a gas turbine, where the pressure difference between inlet and outlet of the cooling channel is limited and dictated by the operating conditions.

As a first step, a parametric study needs to be performed by varying the number of jets per channel and the length transition zone length, as well as by adding a bypass between the channels.

In a second step, heat transfer enhancing features like cross-section reductions, pin-fins, and ribs can be included to improve the heat transfer characteristics of the channel in the transition zone.

By analysing the results of these first two phases, more advanced solutions for heat transfer enhancement will be designed and tested, in order to achieve optimal cooling performances in the transition zone.

Finally, quantitative criteria for the expected impact of these novel cooling solutions on the performances of a gas turbine need to be provided. This is achieved by analysing the complete cycle of a state of the art gas turbine, to estimate the effect of a higher TET and/or a lower coolant massflow on the thermal efficiency of the gas turbine.

2 Description of the test facility

The experimental work is performed in the impingement heat transfer facility of EPFL Group for thermal turbomachinery (Figure 3). The test facility was developed for a previous project in which correlations for narrow impingement channels have been developed based on extensive experimental tests [5].

Figure 3: *EPFL impingement heat transfer facility.*

The main components of the test rig are depicted schematically in Figure 4. Ambient air is sucked by a vacuum pump into a rectangular section via a bellmouth shaped inlet. Downstream of the bellmouth, a honeycomb mesh is installed to ensure one-dimensional flow and to reduce any lateral component of the flow. In the rectangular section, instrumented with static pressure taps and thermocouples, stainless steel meshes (25µm wire diameter, 25% open area) can be used to heat the flow, if

necessary for the applied experimental technique; additionally, these meshes act as screens to reduce the turbulent length scale and ensure uniform flow velocity in the plenum. The actual test channel sits on top of the rectangular section and is also instrumented with pressure taps and thermocouples. A laminar flow element (LFE) is placed between the exit and the vacuum pump to determine the total massflow through the channel. CMOS (Complementary Metal–Oxide–Semiconductor) cameras are used to record the color evolution of the liquid crystals on the impingement surfaces with a resolution of approximately 2.7 pixels/mm and a frame rate of 50 Hz. The static pressure is recorded at various locations of the model, as well as directly upstream and downstream from it, using a pressure scanner (Scanivalve DSA3217), while temperatures upstream of each jet, in both channels, are recorded using type-K thermocouples which were calibrated in a thermostatic bath. The experiment is controlled with a Labview code that reads and records pressure data from the pressure scanner, temperature and voltage data from USB-connected data acquisition modules and controls the power supply via its analog input.

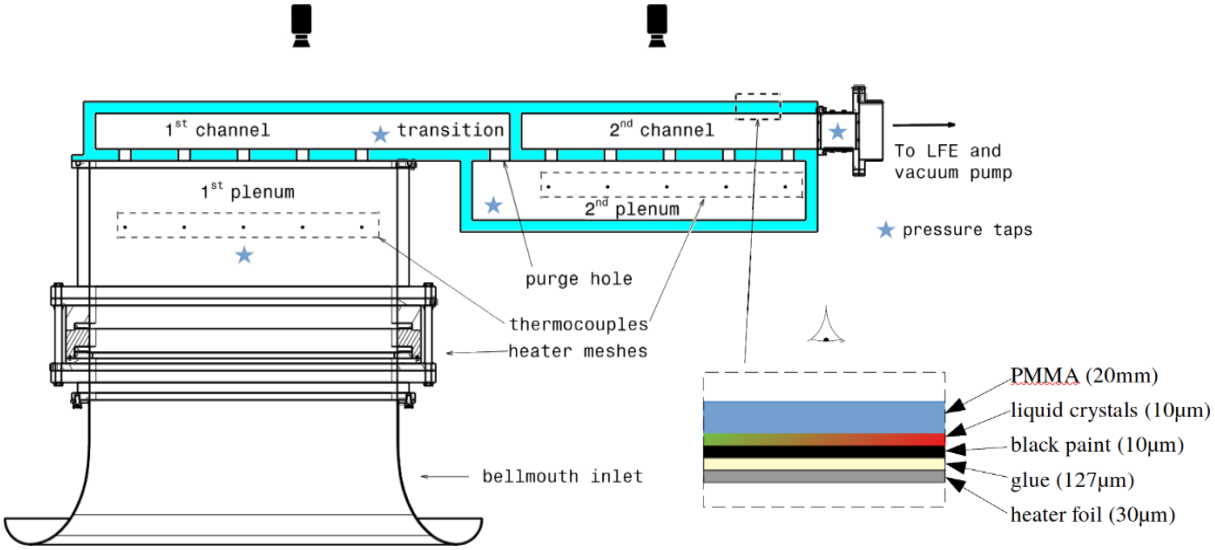

Figure 4: *Schematics of the heat transfer test rig, and instrumentation of the model.*

Several elements have been changed or improved since the last project. The chassis has been extended to allow the mounting of the sequential channels, which are longer and have a second channel placed on the side of the plenum and needs to be supported. The vacuum pump has been replaced and is now more suited to the massflow encountered in this project. Likewise, the laminar flow element (LFE), ensures higher accuracy for the massflow under study. Finally, new digital cameras have been installed to ensure higher frame rate and higher sensitivity.

3 Procedures and methodology

3.1 Experimental technique

The experimental procedure is based on thermochromic liquid crystals (TLCs) applied to the surface under investigation (see Figure 4). TLCs change color depending on temperature, and thus provide information on the temperature, and consequently the heat transfer, in a detailed and non-intrusive way.

A thin layer of TLCs (approximately 10 µm thickness) is sprayed on the surface to be studied, which is made of Plexiglas® (PMMA) to allow for optical access. A thin layer of black paint is sprayed on top of it to improve the contrast of the image acquired with the digital cameras. A heater foil (30 µm thickness) is then applied on the black paint with thermally conductive tape; when a current flows through the foil, a surface heat flux is generated. By using a high resistance material with low temperature coefficient for the foil, it is ensured that the required heat flux is achieved with relatively low values of the electrical current, and that the heat flux is equally distributed across the foil, regardless of the local temperature. In this setup, the internal wall of the channel is painted with TLCs and it is observed through the PMMA.

The technique is transient and relies on a linear increase of the heat flux on the surface. This is a change compared to the technique used in the previous project, where the experiment was driven by a step change in the flow temperature created by the heater meshes in the plenum. The change is required to cope with the fact that some of the geometries to be investigated feature a bypass which is difficult to analyze with a step change in the temperature.

Low bandwidth (1K) TLC are calibrated using an insulated copper bar (see Figure 5), so that the temperature corresponding to the maximum green intensity of the TLC is known. A video recording gives information about the time required for the TLC to reach the green color at each point on the surface. By knowing the thermal properties of the plate and the time required to reach the temperature corresponding to the green color, one can infer the convective heat transfer coefficient of the cooling flow at each location: locations that reach the green color faster have a lower heat transfer coefficient than locations with a slower response time.

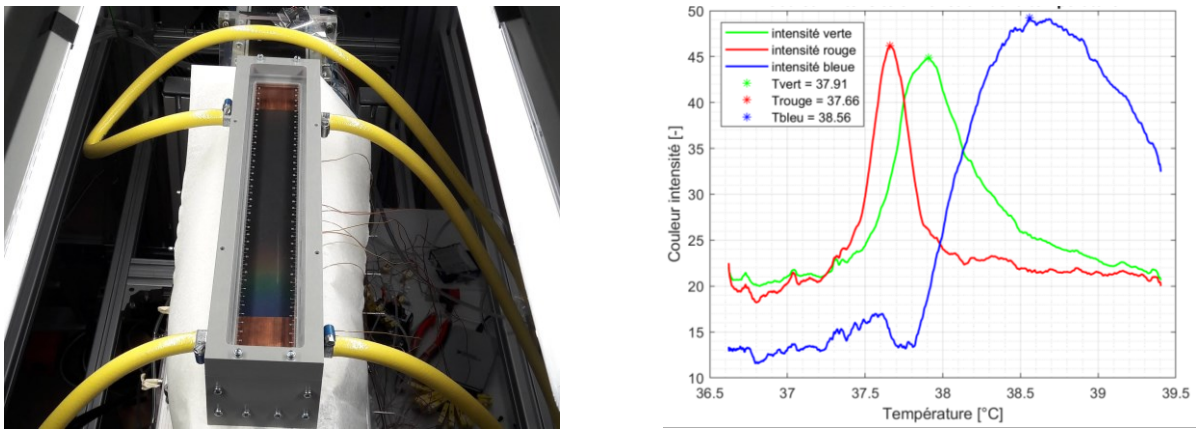

Figure 5: *Insulated copper bar for TLC calibration (left) and example of the resulting calibration (right).*

To determine the heat transfer coefficient several assumptions are made:

- the heat conduction into the solid can be considered one dimensional. Lateral conduction can be omitted with negligible reduction of accuracy for materials having low diffusivity, as is the case for PMMA.
- the plate can be considered semi-infinite. This is a valid assumption if the test duration is shorter than the time required for the heat generated with the heater foil to reach the opposite side of the plate. The plate thickness (20 mm) has been chosen to comply with this assumption.
- the effect of radiation is neglected. This assumption is justified by the fact that the temperatures are low.
- A single material is considered. TLC, paint, and glue are considered to have the same thermal properties of PMMA.

The one dimensional heat equation reads as follows:

$$\frac{\partial^2 T(z,t)}{\partial z^2} = \frac{1}{\alpha}\frac{\partial T(z,t)}{\partial t}$$

where *z* is defined as the depth into the solid from the heated surface, and α is the thermal diffusivity of the solid. According to the aforementioned assumptions, the initial and boundary conditions can be expressed as:

$$T(z,t=0) = T_0 \qquad T(z\to\infty,t) = T_0 \qquad -k\frac{\partial T(0,t>0)}{\partial z} - h[T_{aw} - T(0,t)] = q_0 t$$

In particular, the last expression specifies that at the flow-solid interface (z=0), the applied linearly increasing heat flux $q_0 t$ is equal to the sum of the heat transfer into the solid by conduction (with the thermal conductivity *k*) and the heat convected into the flow (with the heat transfer coefficient *h*).

The equation can be solved analytically leading to the following equation.

$$T(z,t) - T_0 = \frac{q_0}{k\alpha^2}\left[\frac{\alpha}{\left(\frac{-h}{k}\right)^3}\mathrm{e}^{\left(\frac{\mathrm{hz}}{\mathrm{k}}+\mathrm{b}^2\right)}\mathrm{erfc}(a+b) - \frac{\alpha}{\left(\frac{-h}{k}\right)^3}\sum_{r=0}^{2}(-2b)^r i^r \mathrm{erfc}(a)\right]$$

where $a = \frac{z}{2\sqrt{\alpha t}}$ and $b = \frac{h}{k}\sqrt{\alpha t}$ are introduced to simplify the expression, and the term i^r erfc(*x*) represents the rth successive integration of the complementary error function.

The last equation describes the evolution of the temperature as a function of the depth *z* and time *t*. By setting *z* as the depth at which the TLC are placed, *T* as the temperature of the TLCs at the maximum green intensity, and *t* as the time at which the green colour appears, one can solve for the only unknown, the heat transfer coefficient *h*.

The Nusselt number, can be derived directly from the heat transfer coefficient:

$$Nu = \frac{hD}{k}$$

where *D* is the diameter of the jet. The Reynolds number is based on the jet diameter and on the average jet velocity in the 1st channel, and can be expressed in terms of the total massflow $\dot{m}$ as follows:

$$Re_D = \frac{4\dot{m}}{nD\mu\pi}$$

Where *n* is the number of jets in the 1st channel.

The technique is validated on a single jet case installed in a low speed wind tunnel (Figure 6). Results are compared to results from the literature, showing good agreement and an accuracy in the range of 6 to 10%, in line with the previous technique (Figure 7). More information on the implementation and validation of the experimental technique is available in [6].

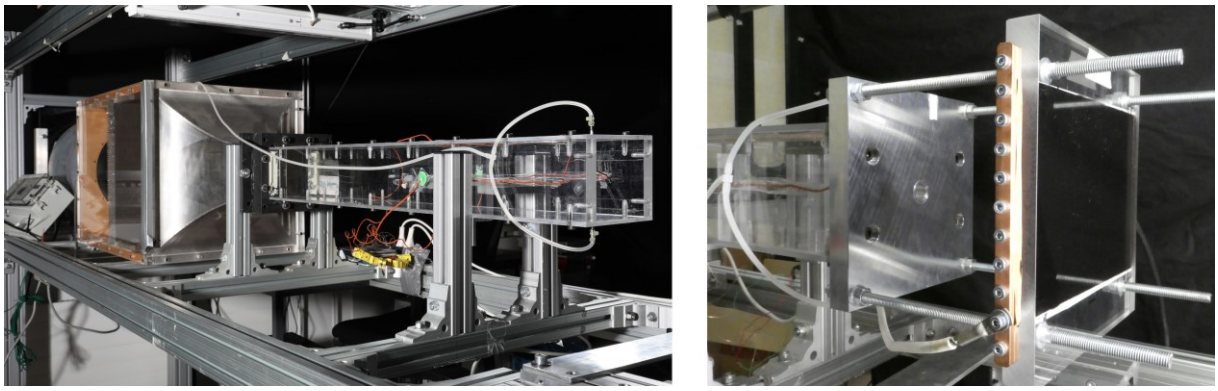

Figure 6: *Linear wind tunnel facility (left), and detail of the single impingement jet experiment mounted at the channel outlet (right).*

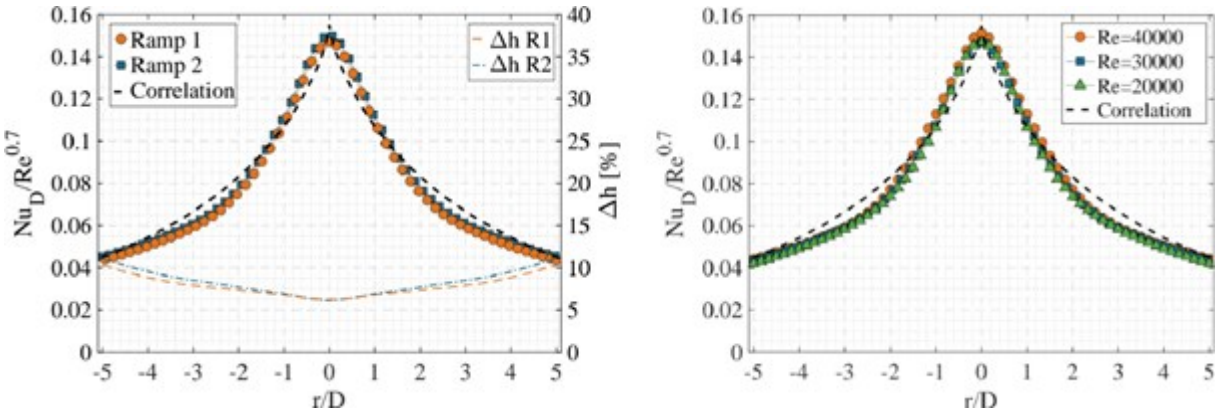

Figure 7: *Left: normalized Nusselt number of a jet with Reynolds number 30000 at a jet to plate distance of 6D, comparison with a correlation from the literature and associated accuracy for two surface heat flux rates of increase (R1 slow, R2 fast). Right: results at a jet to plate distance of 6D and various Reynolds numbers.*

3.2 Test models

The general layout of the cooling channels is depicted in Figure 8; first, the cooling air flows through impingement holes (1) into the first level impingement cavity (2). It then travels through the transition zone (3) and escapes through a purge hole (4) into the second plenum (5). It can then pass through the second level impingement holes (6) into the second level impingement channel (7) before discharging (8).

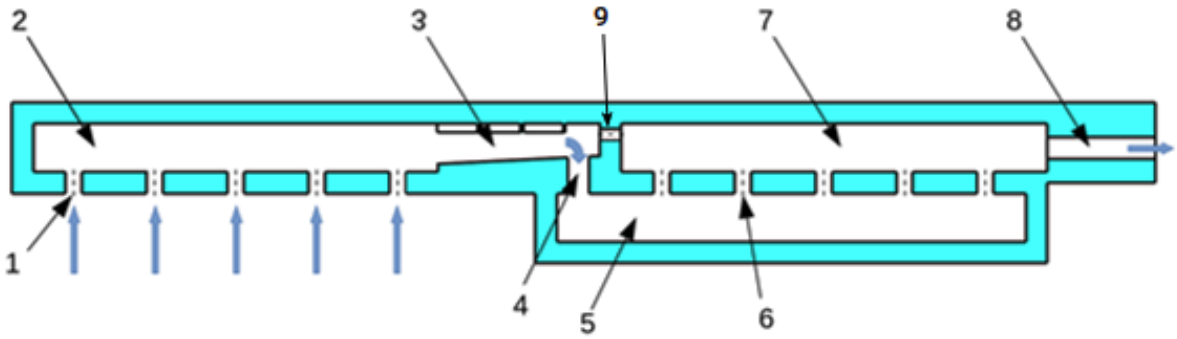

Figure 8: *Schematic view of the sequential impingement channel.*

Figure 8 also includes heat transfer enhancing features that are to be studied in this project, and which are located in the transition zone (3). Ribs can be installed on the target plate, the cross-section of the channel can be reduced in the transition zone by inserting a ramp on the jet plate, one or multiple bypass holes (9) can be included that allow part of the massflow to pass directly from the first channel to the second channel. Additionally, pin-fins can be included in the transition zone (not pictured in Figure 8), and the length of the transition zone itself can be varied.

The models are built using 20 mm thick PMMA plates (10 mm thick for some parts), and are designed in a modular way, so that a minimum of parts need to be changed from one configuration to the next.

3.3 Test matrix

All geometries tested have a channel width Y equal to 5D (D being the jet diameter), and a jet-to-plate distance Z=3D. All geometries but one have a jet-to-jet spacing X of 5D, with the only exception being geometry 5505XD3 which has a jet-to-jet spacing of 3D in the first channel. The purge hole has a surface area equal to two times the total jet hole area of the first channel of the baseline case. In total, 35 geometries have to be tested at three engine relevant Reynolds numbers of 10000, 20000, and 40000. The table below lists the values of the varying parameters, which are the number of jets in the 1st and 2nd channel, the length of the transition zone, and the addition of heat transfer augmentation features, which are generally implemented in a channel with the same geometry as the baseline, with some exceptions for the bypass cases which feature a shorter transition zone.

The table also shows the codename attributed to the geometries, in which the first two numbers indicate the number of jets in each channel while the 3rd and 4th number indicate the transition zone length; in case of enhancing features, a combination of letters and numbers is appended to the codename.

Name	# holes 1st channel	# holes 2st channel	Transition length	Enhancing features
5510	5	5	10D	None, “baseline geometry”
5505	5	5	5D	None
5515	5	5	15D	None

7505	7	5	5D	None
7510	7	5	10D	None
7705	7	7	5D	None
7710	7	7	10D	None
5505B1	5	5	5D	Central bypass
5505B2	5	5	5D	2 lateral bypasses
5510R1	5	5	10D	Short ramp, height 2D
5510R2	5	5	10D	Long ramp, height 2D
5505XD3	5	5	5D	Shorter jet-to-jet spacing (X/D=3)
5510BR	5	5	10D	Baseline ribs (inclined ribs 45°)
5510VR45	5	5	10D	V-ribs 45°, 1st rib upstream of last jet
5510VR45B	5	5	10D	V-ribs 45°, 1st rib downstream of last jet
5510VR45R	5	5	10D	V-ribs 45° + short ramp, height 2D
5510VR60	5	5	10D	V-ribs 60°,1st rib upstream of last jet
5510VR60B	5	5	10D	V-ribs 60°, 1st rib downstream of last jet
5510CR45	5	5	10D	Chevron ribs 45°
5510DV45	5	5	10D	Discrete V-ribs 45°
5510DV45BP	5	5	10D	Discrete V-ribs 45° + central bypass
5510DV60	5	5	10D	Discrete V-ribs 60°
5510VP	5	5	10D	Vertical pin-fins (baseline pins)
5510VPS	5	5	10D	Small vertical pin-fins
5510IP	5	5	10D	Inclined pin-fins
5510PR	5	5	10D	Pin-ribs
5510PRBP	5	5	10D	Pin-ribs + bypass
5510B4	5	5	10D	4 bypasses
5510DCR	5	5	10D	Discrete chevron ribs
5510DCRR	5	5	10D	Discrete chevron ribs short ramp, height 1D
5510DCRR1	5	5	10D	Discrete chevron ribs short ramp, height 2D
5510DVRR	5	5	10D	Discrete V-ribs short ramp, height 1D
5510DVRR1	5	5	10D	Discrete V-ribs short ramp, height 2D
5510PRR	5	5	10D	Pin-ribs, with short ramp, height 1D
5510RS	5	5	10D	Short ramp, height 1D

4 Results and discussion

4.1 Heat transfer results

To report the main findings of the experimental campaign, in this section selected heat transfer results are analysed in detail, while the Nusselt number plots on the target plates for all the configurations tested are provided in Annex 1.

4.1.1 Baseline geometry

The baseline geometry (5510) features 5 jets per channel and a 10D long transition zone. Nusselt number distributions on both plates are shown in Figure 9 for the case Re=10000. Both channels have similar Nu values, but one has to keep in mind that in a real case scenario, the cooling air temperature in the second channel is higher than in the first, leading to a lower cooling capacity. The transition zone (right part of Figure 9) experiences very low levels of heat transfer, which can create issues with the thermal stresses associated with the large temperature gradients arising in the material. Both channels show the maximum heat transfer at the stagnation point of the 4th jet: this means that the difference in the flows between 1st and 2nd plenum does not play a crucial role.

In Figure 10, Nu data in the centerline are normalized by $Re^{0.7}$, a factor commonly used for this type of channels to compare different Reynolds numbers. Results show that heat transfer data at different Reynolds numbers scales well with this factor, in line with previous findings for single channels [5]. Only in the stagnation region, where the flow is laminar and Nu scales with $Re^{0.5}$, a discrepancy can be observed. At higher Reynolds numbers (Re=20000 and Re=40000), the highest Nu is achieved at the 5th jet in the 1st channel, while the relative intensity in the second channel is similar between Reynolds numbers.

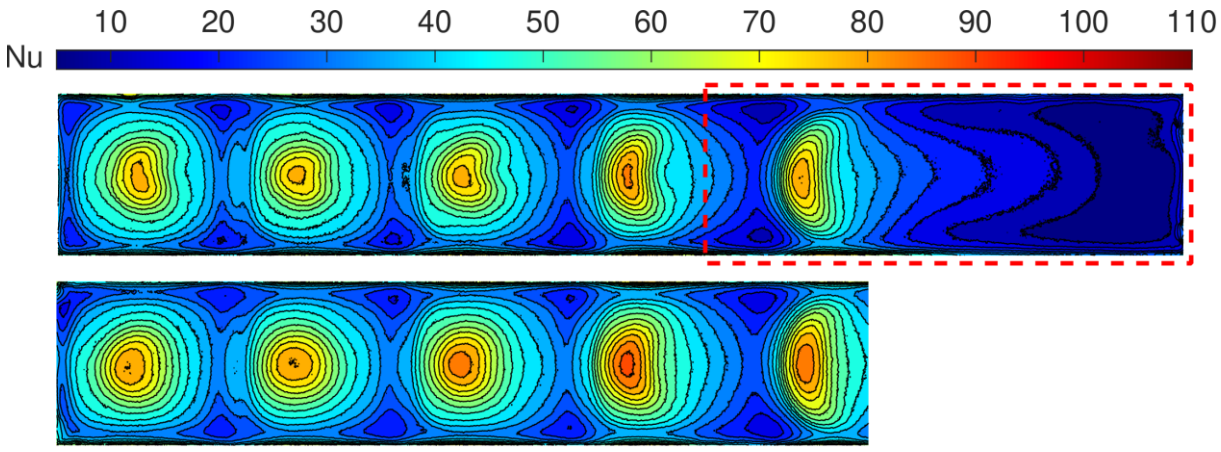

Figure 9: *Nusselt number distribution on the 1st (top) and 2nd (bottom) channel for case 5510 (baseline case) with 5 jets per channel and a transition zone of 10D. Re=10000. The dashed red rectangle represents the area used for the detailed analysis of the transition zone heat transfer.*

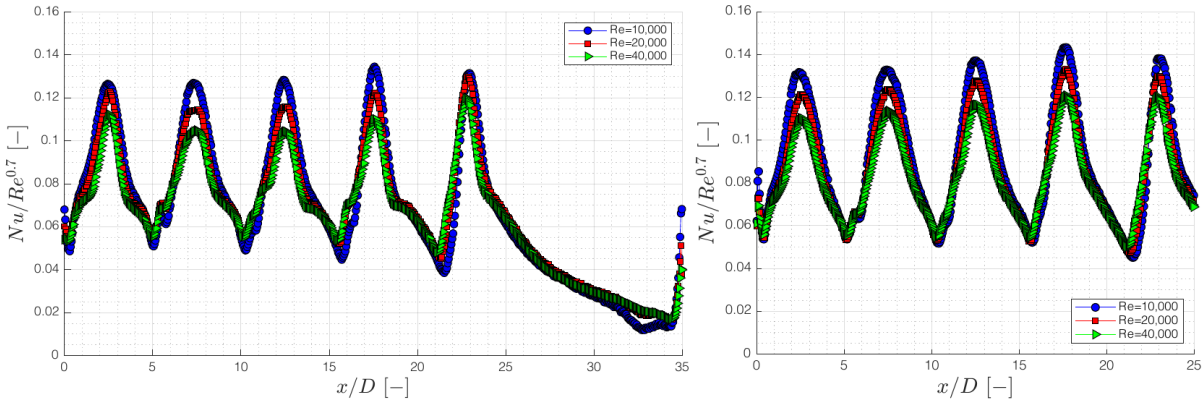

Figure 10: *Nu values divided by $Re^{0.7}$ in the centerline of the 1st (left) and 2nd (right) channel for the geometry 5510 at various Reynolds numbers.*

4.1.2 Variation of the number of holes

Tests have been carried out on channels with 5 and 7 holes in both channels. Figure 11 shows the centerline (left) and spanwise-averaged (right) normalized Nusselt values for geometries with 5 holes in both channels and 7 holes in both channels at Re=20000. For impingement jets 1-5 the results are independent on the total number of holes, which is consistent with the findings in [7]. Heat transfer at the stagnation point for holes 6-7 is slightly lower than jets 4-5, due to the crossflow. Since tests are carried out at equal jet Reynolds numbers, the average flow velocity is higher in the transition zone for the 7 holes configuration (due to the higher total mass flow), leading to higher Nu values in the transition zone.

Geometries with 7 jets in the first channel and 5 in the second were also tested (7505 and 7510). In this case, since the Reynolds number is based on the average jet velocity in the first channel, Nusselt values in the second channel are higher due to higher jet Re, but also the pressure difference needed to drive the flow is higher, due to the smaller passage area in the second channel. Since the flow temperature in the second channel is higher than in the first, less cooling capacity is foreseen, which could be mitigated by having higher flow velocity in the 2nd channel.

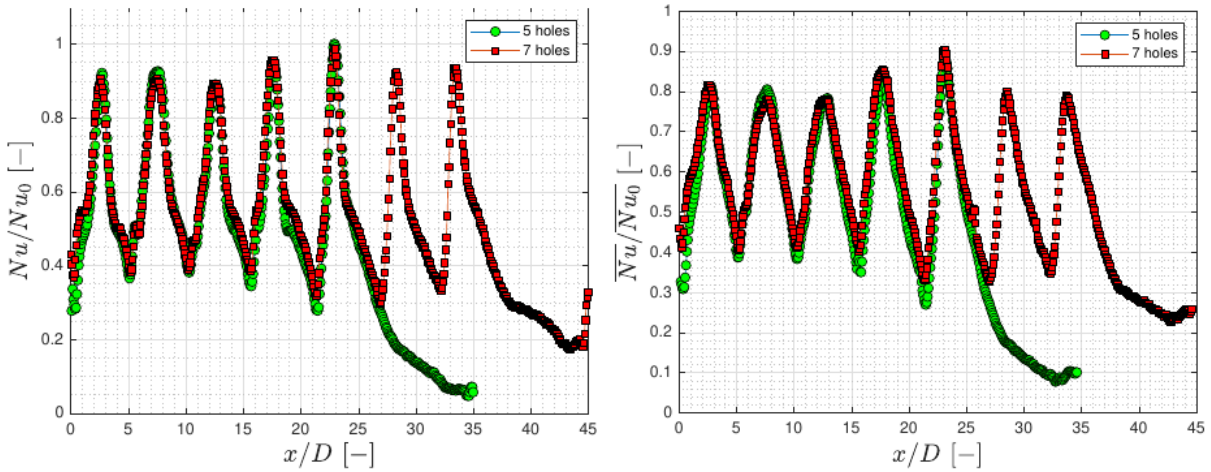

Figure 11: *Centerline (left) and spanwise-averaged (right) Nu, normalized with the maximum value in the 1st channel, for a geometry with 5 jets (5510, baseline, green) and a geometry with 7 jets (7710, red). Re=10000.*

4.1.3 Variation of the length of the transition zone

When decreasing the length of the transition zone (geometry 5505, L_{trans} = 5D), a secondary impingement of the wall jet flow to the endwall of the channel can be seen in the Nusselt distribution in Figure 12 (top plot). The short transition shows a similar spanwise-averaged distribution as the baseline transition (L_{trans} = 10D), while the longer transition zone (geometry 5515, L_{trans} = 15D) shows a slower drop in the Nusselt number, due to the flow remaining attached to the target plate for a longer distance, before being discharged through the purge hole on the opposite side of the channel (Figure 13).

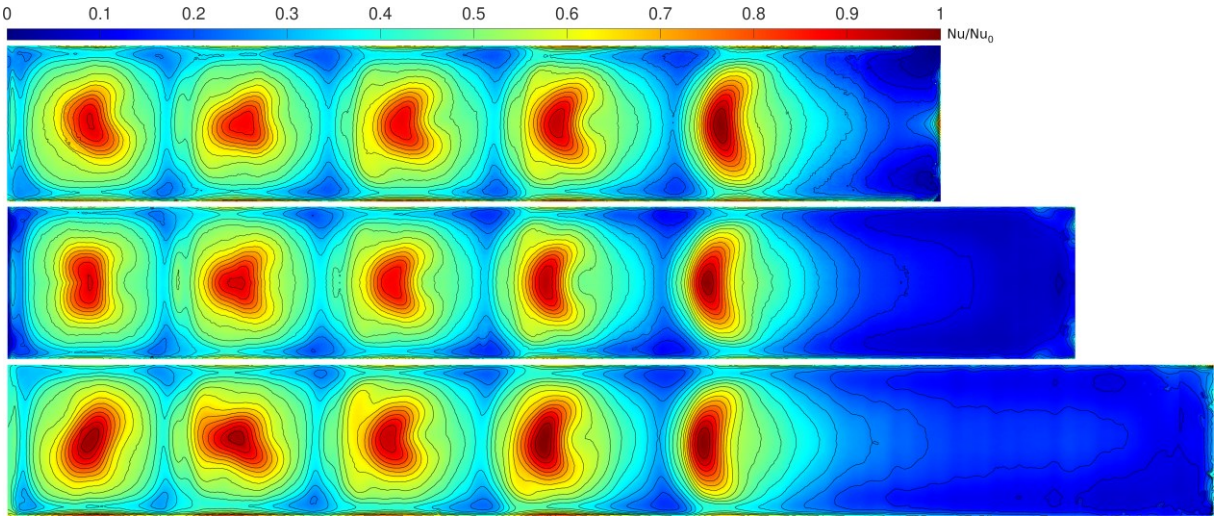

Figure 12: *Nu distribution, normalized with the maximum value in the baseline geometry (5510), in the 1st channel for 3 different length of the transition zone. From top to bottom, geometry 5505 (L_{trans}=5D), 5510 (L_{trans}=10D, baseline), 5515 (L_{trans}=15D) at Re=20000.*

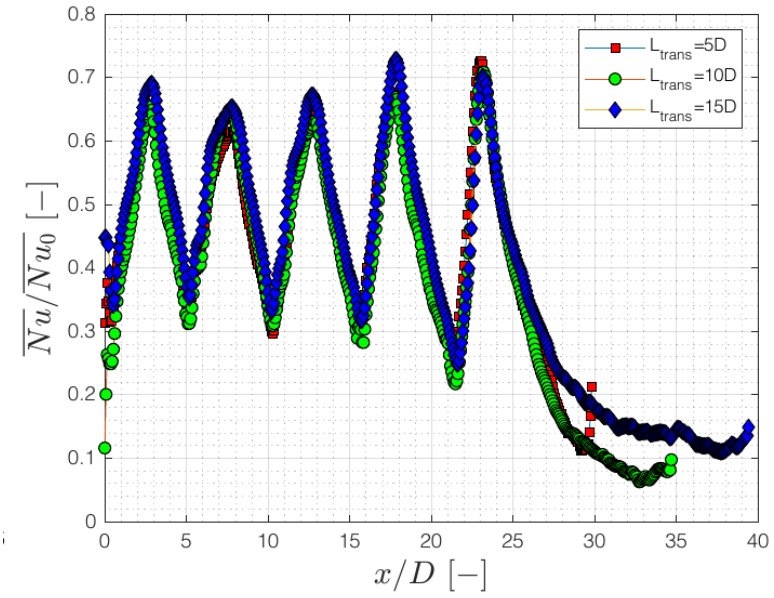

Figure 13: *Spanwise-averaged data of Figure 12.*

4.1.4 Addition of a bypass

A bypass can be added to allow some of the flow to pass directly from the 1st channel to the 2nd. This can bring some benefits to the overall performances of the cooling channel:

- The passage area between 1st and 2nd channel is increased, potentially decreasing the pressure losses of the flow.
- The flow in the upstream part of the 2nd channel is modified, with the bypass flow providing enhanced heat transfer in this region.

Three layouts of the bypass holes are tested; in all cases the bypass is placed as close as possible to the target plate. Configuration 5505B1, 5505B2 and 5510B4 have 1 central bypass hole, 2 bypass holes place at 1/3 and 2/3 of the width, and 4 bypass holes at 1/5, 2/5, 3/5 and 4/5 of the width, respectively. In all cases the total bypass area is equal to 1/2 of the jet hole area.

Results on the 1st channel show no noticeable effect of the bypass on the Nusselt number distribution. In the second channel, the addition of bypasses causes important changes in the Nu distributions (Figure 14). First, the bypass flow is essentially a jet flow parallel, and very close to, the target surface. This creates a local Nu increase. In between the jets, however, the bypass flow disturbs the wall jet flow of the 1st impingement jet, and causes a drop in the Nu between the bypass jets, or in the case of the single bypass case, left and right of the jet. This effect is mitigated by increasing the number of bypass jets, as can be seen in the case of 4 bypasses.

Since some of the flow is bypassed, the average jet velocity in the second channel is lower; this translates in lower Nu values at the jet stagnation point (see also Figure 15). The higher crossflow to jet flow ratio for the bypass cases results in an increased interaction of the crossflow with the jets, leading to less round shape in the Nu distribution and a shift downstream of the stagnation point (see the last jet). Additionally, the 1st jet is highly impacted by the bypass, leading to lower heat transfer, especially in the single bypass case where the bypass is aligned with the jet, and a deformed Nu pattern around the stagnation region (2 bypass case in particular).

The 4 bypass case has increased values of the average Nu upstream of the 1st jet, and sees the least amount of reduction of the heat transfer in the impingement region. Thus, it seems that increasing the number of bypass holes improves the performances of the channel. However, if one aims to keep the total bypass area constant, the holes become smaller, and the manufacturability of such a feature will become challenging.

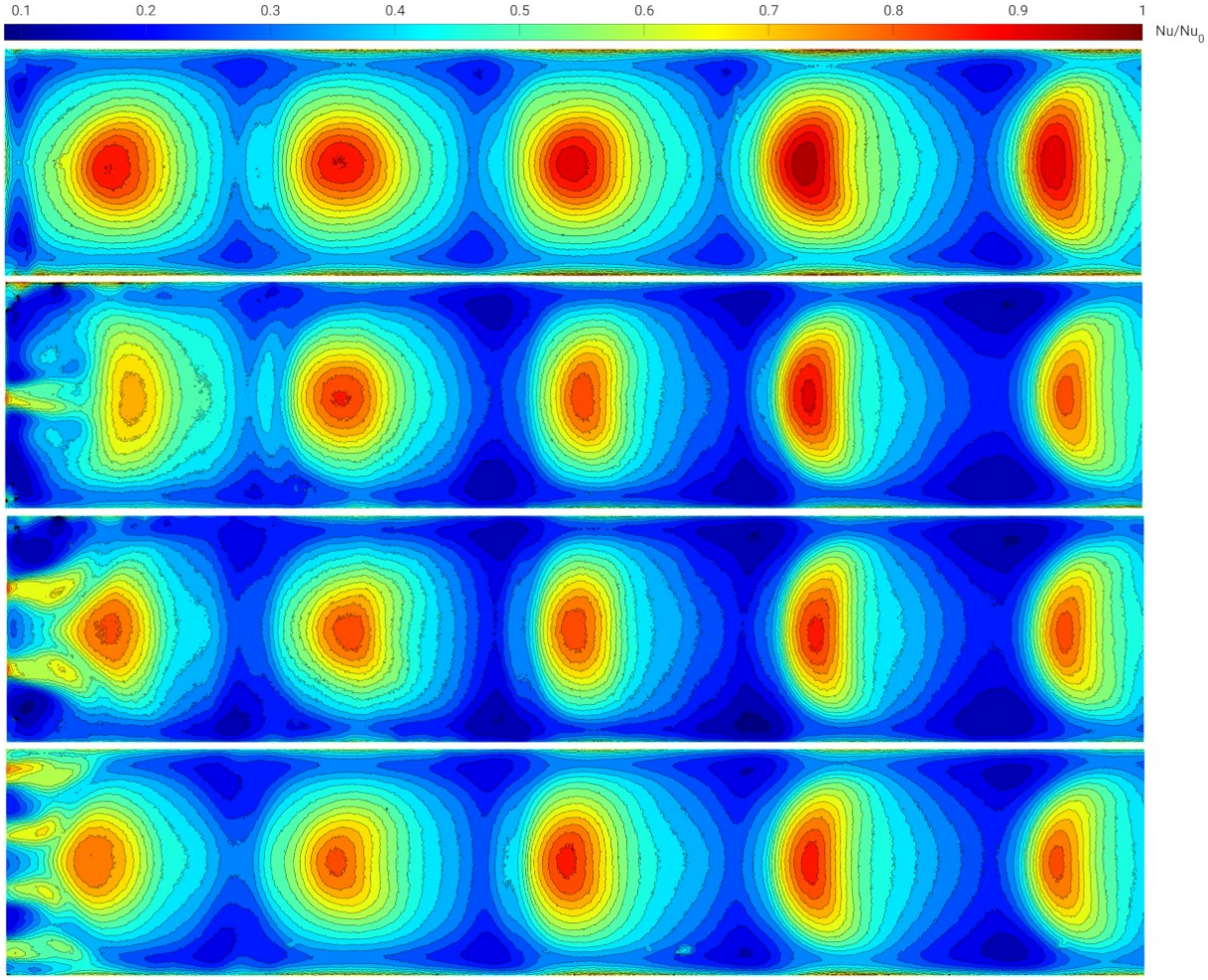

Figure 14: *Nu distribution in the 2nd channel, normalized with its maximum value, for cases 5505, 5505B1 (single bypass), 5505B2 (2 bypass holes), 5510B4 (4 bypass holes). Re=10000.*

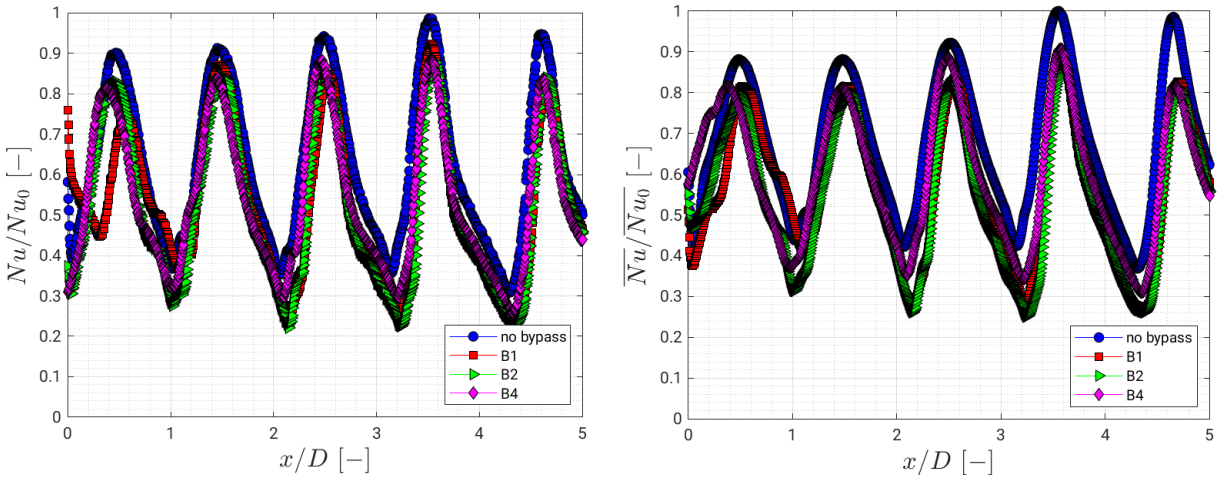

Figure 15: *Spanwise-averaged distribution of the data of Figure 14.*

4.1.5 Ramps

The addition of ramps in the transition zone, on the jet plate side, has the objective of increasing the flow velocity, and thus the heat transfer, in this region.

Two types of ramps are studied. The short version (Figure 16, left) ends with a round corner at the beginning of the purge hole, while the long version (Figure 16, right) ends at the end of the channel. Ramps have a slope of 30° until the specified maximum length and a constant height afterwards. The height of the ramps is 2D, where D is the jet diameter, leaving an open height of 1D for the channel. A smaller version (height=1D) of the short ramp is also studied; the bigger open area of this version could allow the addition of ribs on the opposite side.

Results (Figure 17 and Figure 18) show, as expected, an increase of the heat transfer in the transition zone, with the longer version of the ramp reaching higher Nu than the shorter version, but with a penalty in terms of pressure losses (see Section 4.2). The small, short ramp still achieves some improvement of the heat transfer, with an increase of the average Nu in the transition zone of 7.5% for the Reynolds number shown in Figure 17.

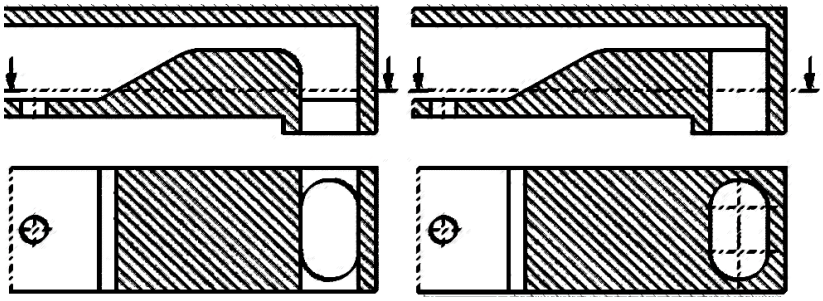

Figure 16: *Schematics of the short (left) and long (right) ramp.*

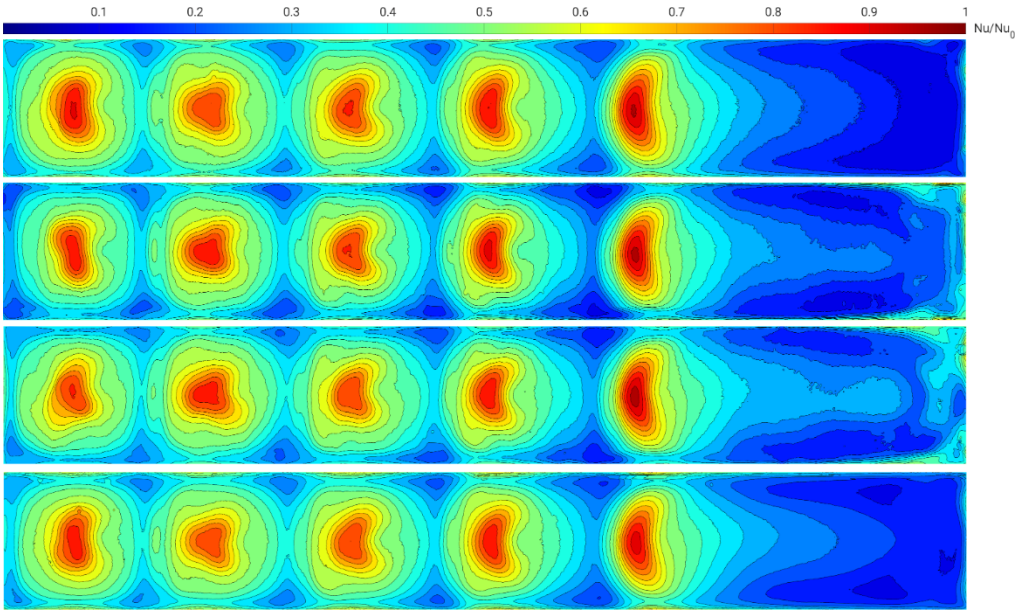

Figure 17 *Normalized Nu for the case (from top to bottom) 5510 (baseline), 5510R1 (short ramp, height=2D), 5510R2 (long ramp, height 2D), 5510RS (short, small ramp, height=1D). Re=20000.*

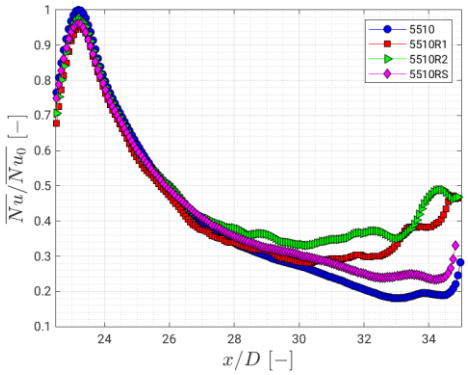

Figure 18: *Spanwise-averaged data of Figure 17, for the region inside the red rectangle of Figure 9 (last jet and transition zone), Re=20000.*

4.1.6 Ribs

Placing the ribs on the target plate promotes a detachment of the boundary layer and a mixing with the (colder) main flow, which improves the heat transfer downstream of the rib. In this project, 5 types of ribs are studied (Figure 19): inclined ribs, V-ribs, chevron ribs, discrete V-ribs and discrete chevron ribs. They are always installed in the baseline geometry (5510).

All ribs have a square section of side 0.45D and are placed at 45° from the channel axis. Some ribbed configurations are also tested with an angle of 60°.The discrete version of the ribs is also tested with the short ramp, to further enhance the heat transfer capabilities.

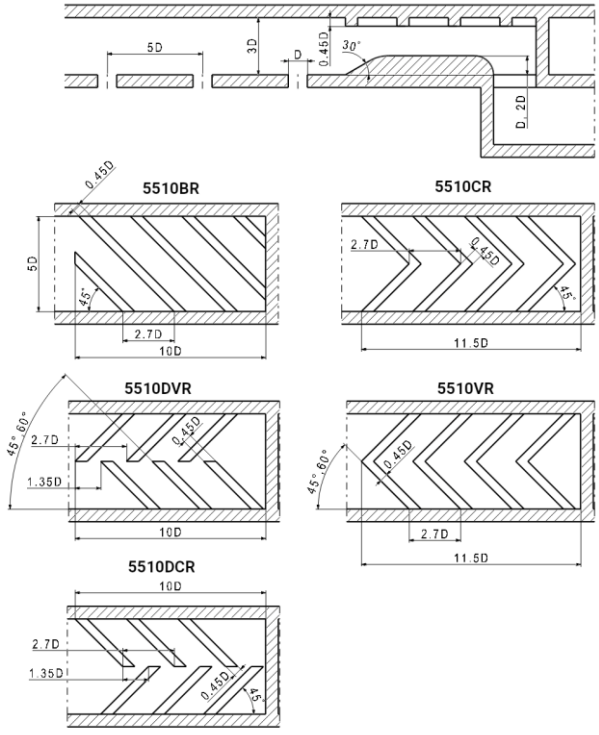

Figure 19: *Schematics of the ribbed configurations.*

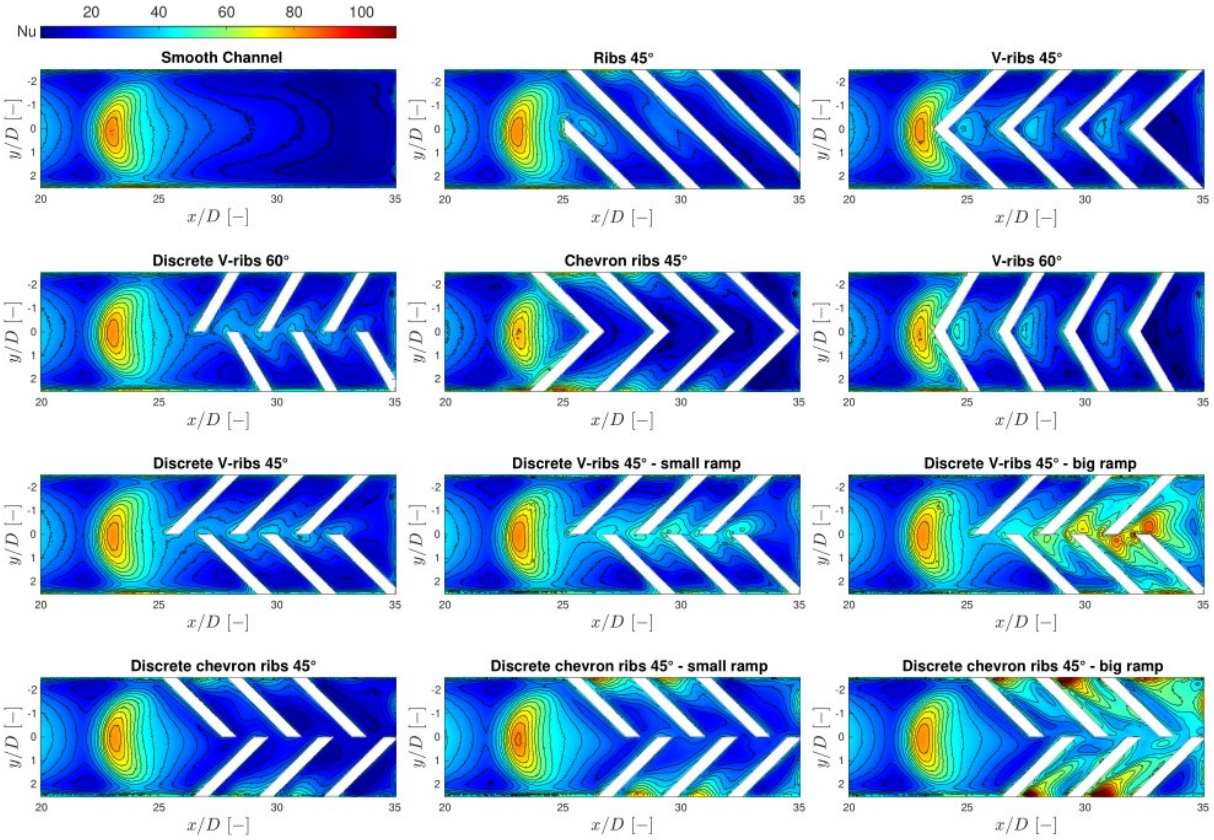

Figure 20: *Nusselt number distribution of the ribbed configurations at Re=10000. The visualization is limited to the region inside the red rectangle of Figure 9.*

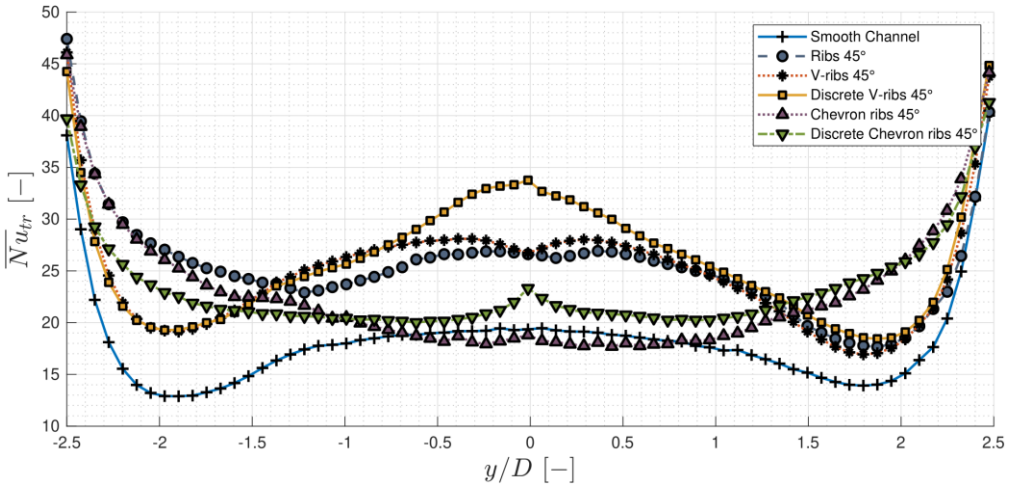

Figure 21: *Streamwise-averaged Nu of some of the ribbed configurations at Re=10000. The averaging is limited to the transition zone.*

Figure 20 presents the Nusselt number for the investigated ribbed configurations; only the last impingement jet of the first channel and the transition zone are shown, corresponding to the red rectangle in Figure 9. All ribs allow for an increase of Nu values in the transition zone, with the V-ribs providing an increase in the central part of the transition zone, while the chevron ribs increase the Nu near the sidewalls; this is due to the different rotation direction of the vortices generated by the ribs [8], which move cool air from the mainstream to the target plate. This effect can be seen more clearly in Figure 21, where the streamwise averaged Nu values of the transition zone are shown for all 45° ribs without cross-section reduction.

The last jet of channel 1 is in most cases largely unaffected by the ribs. Only the V-ribs (especially at 60°) and the chevron ribs, due to their proximity with the last jet, interact with the jet flow near the stagnation region, changing the shape of the heat transfer pattern of the jet; however, this does not have a significant impact on the overall heat transfer in the stagnation area of the last jet.

Discrete V- and chevron ribs are obtained by moving one half of the ribs half a pitch downstream, away from the last jet stagnation point, and have 3 rows of ribs instead of 4. This reduces the interaction with the last jet and avoids the reduction of the peak heat transfer at the stagnation of the last jet. In the case of the chevron ribs, however, this somewhat reduces the heat transfer enhancement near the sidewalls since the first rib is less affected by the wall jet flow.

By looking at the area averaged Nu in the transition zone (Figure 22), the geometries can be grouped into 4 categories: 1) the baseline geometry (smooth channel); 2) the ribbed geometries without cross-section reduction, which improve the average Nu by 10% to 45%, depending on Re and configuration; 3) the configurations with a small cross-section reduction, which improve Nu values by 40% and 75%; 4) the configurations with a big cross-section reduction, which improve the Nu between 80% and 138%. In all cases, the percentage increase is highest at Re=10000 and lowest at Reynolds=40000; this is mainly due to the fact that the increase in absolute terms is similar for all Reynolds numbers.

The ribbed geometries without cross-section reduction show different performances between each other depending on the Reynolds number considered; it is however to be noted that the difference between configurations is often within the accuracy of the applied experimental method. However, discrete V-ribs (both angles) are consistently the top performers; only at Re=40000 the configuration with V-ribs 60° is better. This configuration also shows a different Reynolds scaling than the others, probably due to the different angle of the ribs generating a different flow topology.

The discharge through the purge hole, on the opposite side of the channel, reduces the efficiency of the last rib, which causes a reduction of the spanwise averaged Nusselt number near the end of the channel, followed by an increase which can be attributed to a secondary impingement on the end wall.

As seen in the previous section, the reduction of the cross-section by means of a ramp causes an increase of the mean Nu in the transition zone. This is also the case for the ribbed configurations, and this can be seen more clearly in Figure 23, where the spanwise-averaged Nu is plotted for the discrete chevron ribs and discrete V-ribs configurations for the region included in the dashed rectangle of Figure 9. For the big ramp, the heat transfer in the transition zone is comparable to the last impingement jet. There is however a price to pay for this performance in terms of pressure losses, because the passage area in this case is very small, with a free channel height reduced to 0.55D (the channel height without ramp is 3D). The small ramp provides a bigger free channel height (1.55D) which is much more favorable for the pressure losses, and the heat transfer is moderately increased compared to the baseline, with a spanwise-averaged value roughly constant along the transition.

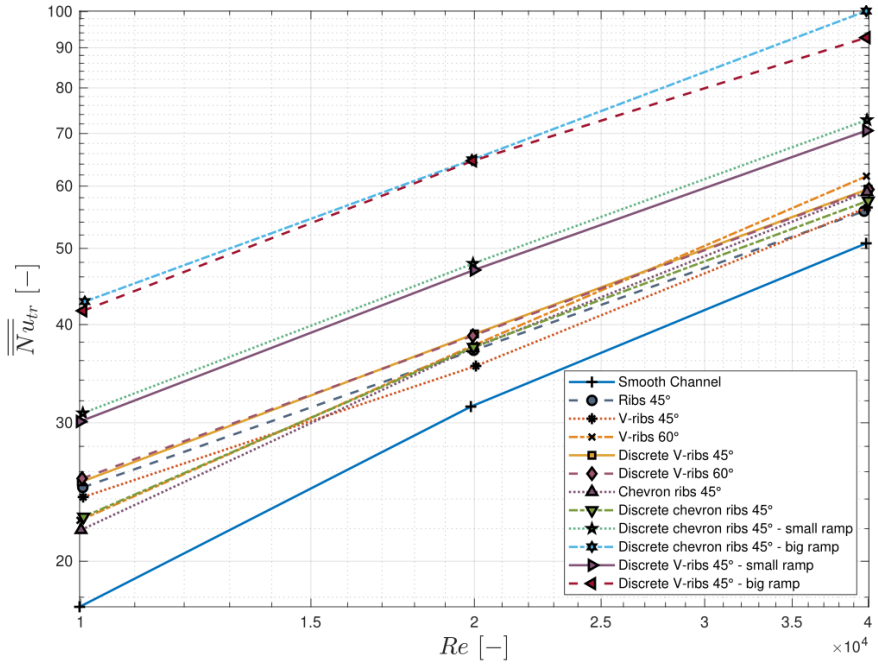

Figure 22: *Area-averaged Nu in the transition zone as a function of the Reynolds number for the ribbed configurations.*

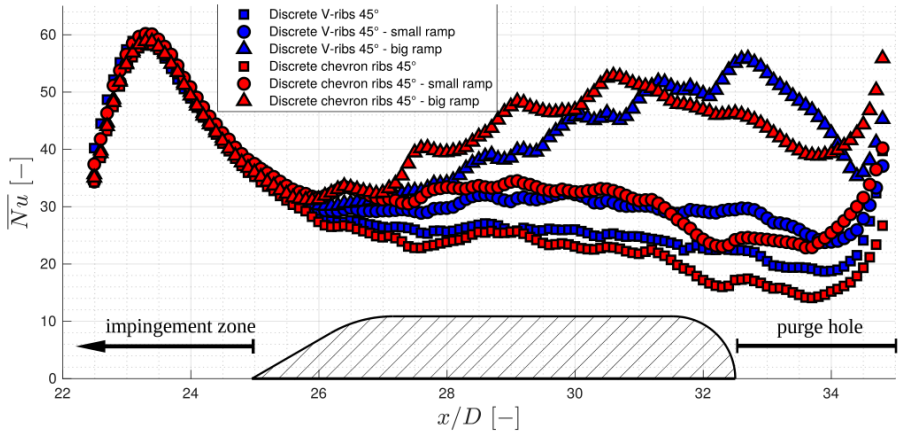

Figure 23: *Spanwise-averaged Nu for the discrete ribs configurations with and without ramps at Re=20000.*

4.1.7 Pin-fins

Four geometries with pins have been studied (see Figures Figure 24Figure 27): staggered vertical pins of diameter 1D, staggered vertical pins of diameter 0.5D, inclined pins of diameter 1D with alternating rows and staggered vertical pins of diameter 1D with ribs connecting them.

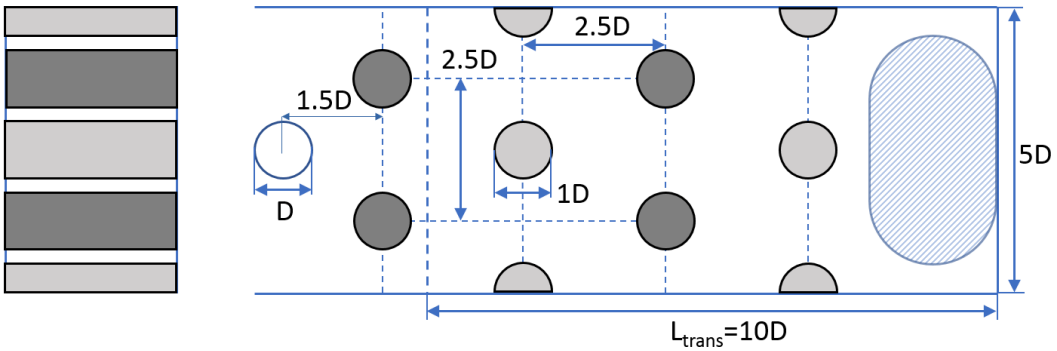

Figure 24: *Schematics of the vertical pins configuration.*

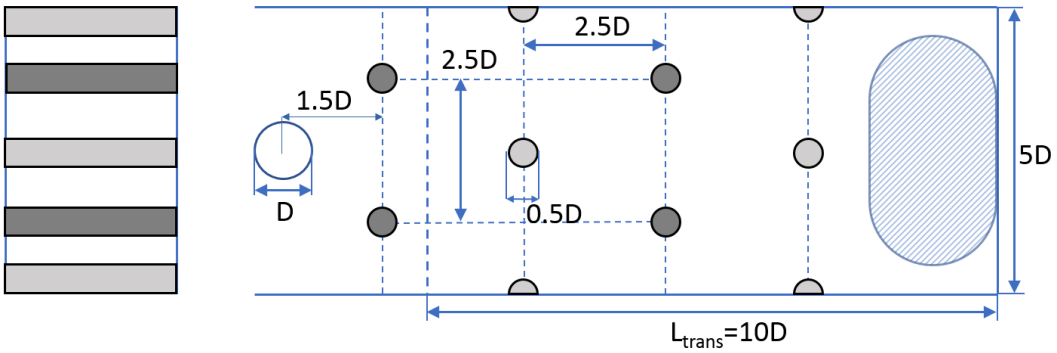

Figure 25: *Schematics of the small vertical pins configuration.*

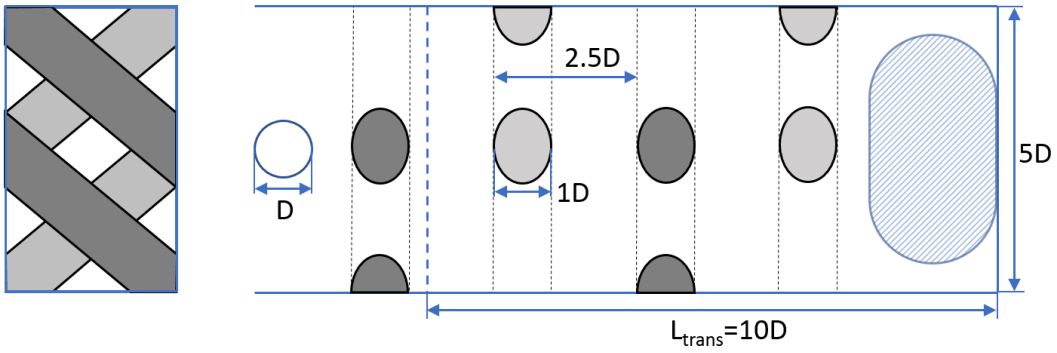

Figure 26: *Schematics of the inclined pins configuration.*

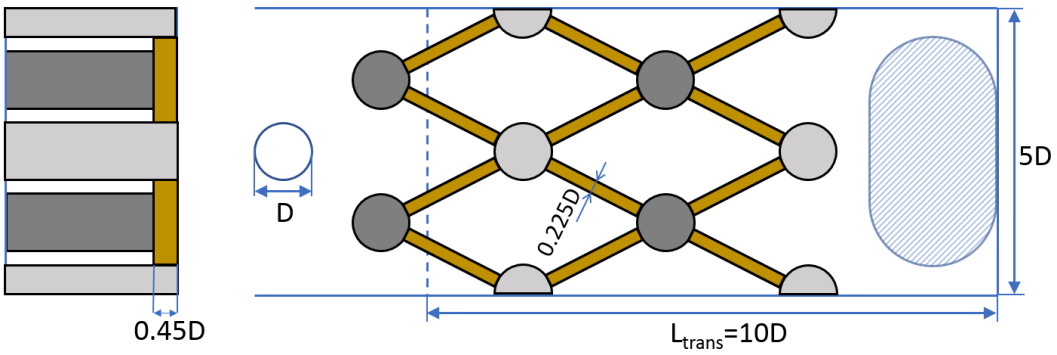

Figure 27: *Schematics of the pin-ribs configuration.*

Figure 28 shows the Nusselt number for the smooth geometry and all the pin-fins cases at Re=20’000. For the vertical pins case, an improvement of the heat transfer coefficient can be seen downstream of the pins. The first row of pins is very close to the last jet impingement area, which is about 0.5 jet diameters downstream of the jet position due to the crossflow of previous jets. It is debatable if this placement improves the overall heat transfer, since heat transfer data on the pin itself is not available. At the end of the plate, a low heat transfer region can be seen, which is due to the flow turning towards the purge hole, leaving a zone with detached, recirculating low speed flow near the target plate. When reducing the pin diameter, similar observations can be made, but the beneficial effect of the pins is reduced. A fairer comparison could be made by keeping the total frontal area of the pins constant (i.e. having 4 pins instead of 2 for each row).

Inclined pins lead to an increase of the heat transfer coefficient both upstream and downstream of the pin. The Nusselt number patterns are more complex in this case and asymmetrical due to the asymmetric geometry configuration. The low heat transfer region at the end of the plate is reduced, but is still low on one side of the plate (lower side in the figure).

For the pin with ribs configuration, the highly complex flow field arising from the interaction of pins and ribs creates regions of high heat transfer between the ribs.

Figure 29 shows the spanwise-averaged normalized Nusselt number for the first channel. In all cases the enhancement features interact with the last jet impingement zone reducing slightly the heat transfer values near the stagnation zone. The small vertical pins produce only a marginal improvement in the transition zone, while reducing the heat transfer at the end of the plate, as noted previously. Bigger vertical pins show a more substantial improvement in the transition zone. Pin-ribs improve the heat transfer even more. Finally, inclined pins show even higher heat transfer, slightly better on average than the pin-ribs.

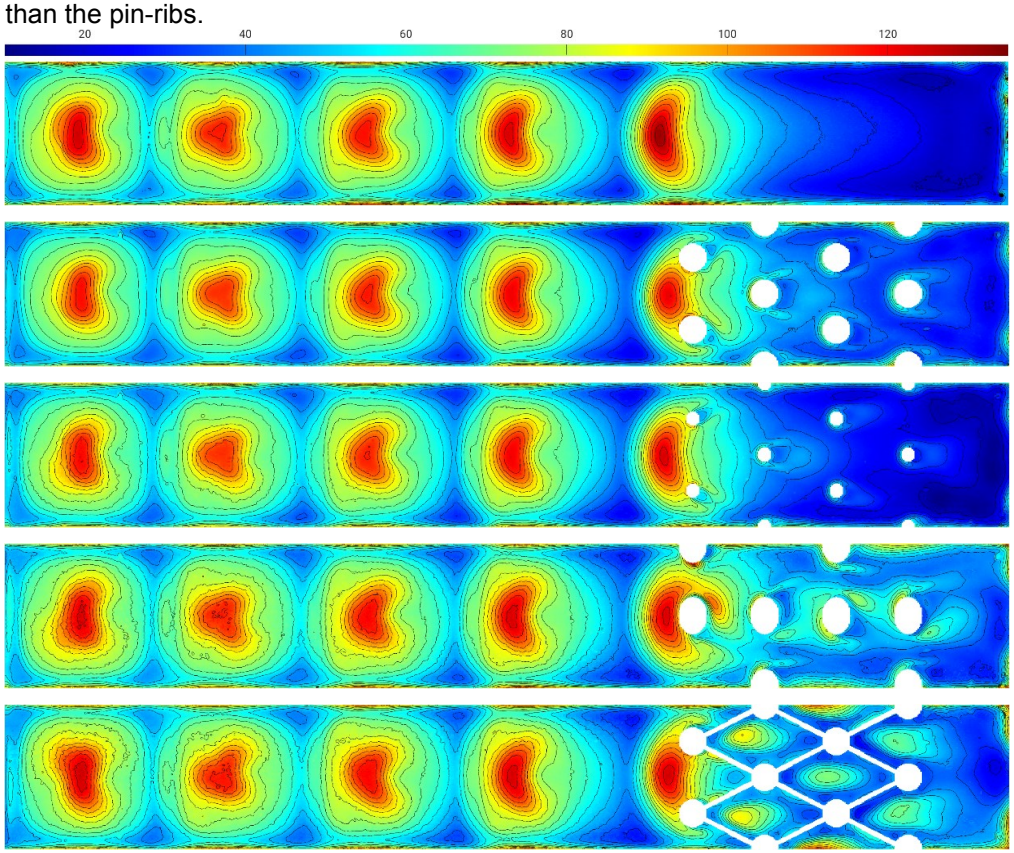

Figure 28: *Nusselt number distribution on the target plate for the 4 configurations. From top: smooth channel (baseline, 5510), vertical pins (5510VP), small vertical pins (5510VPS), inclined pins (5510IP) and pin-ribs (5510VP) at Re=20000.*

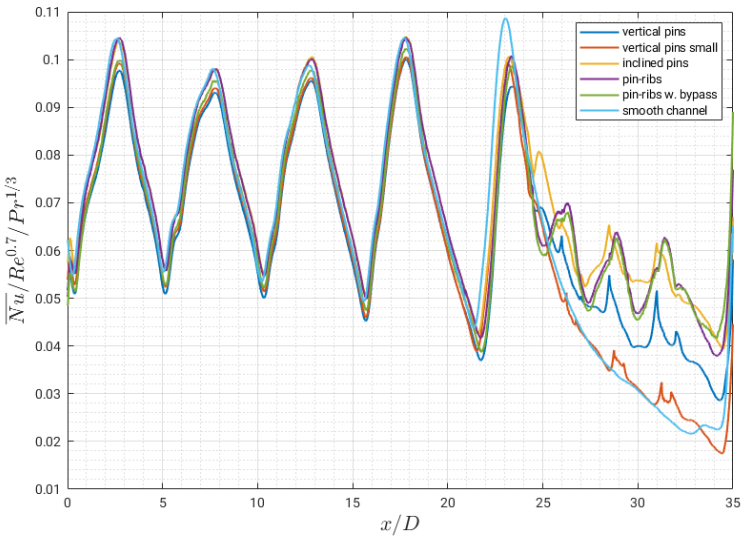

Figure 29: Spanwise-averaged normalized Nusselt number for the various configurations tested.

4.1.8 Combined configurations

Based on lessons learned in the experimental campaign, additional configurations have been tested, trying to combine the beneficial effect of different heat transfer enhancement strategies. In particular discrete chevron and discrete V-ribs have been combined with ramps (results presented in Section 4.1.6) and pin-ribs combined with the small ramp (height=1D). Results for the latter are shown in Figure 30 and Figure 31. The inclusion of the ramp increases noticeably the Nu values between the ribs, as well as at the end of the channel, with a small penalty in terms of pressure losses, as will be discussed later in the report.

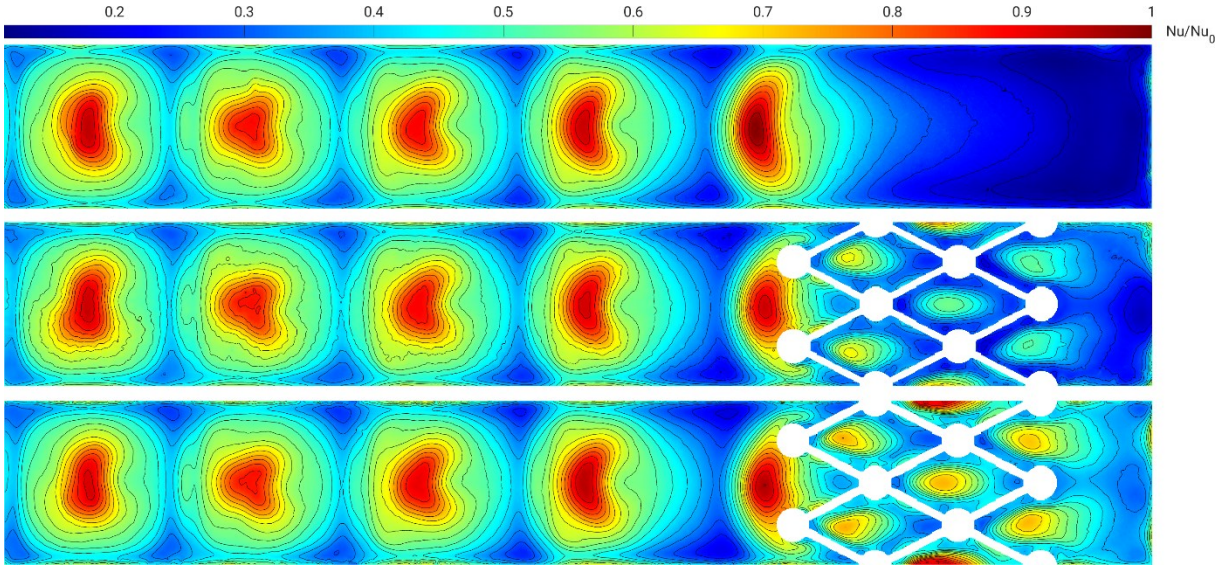

Figure 30: *From top to bottom smooth geometry (5510), pin-ribs geometry (5510PR) and pin-ribs geometry with small ramp (5510PRR) Nu values normalized with the maximum value in the smooth geometry.*

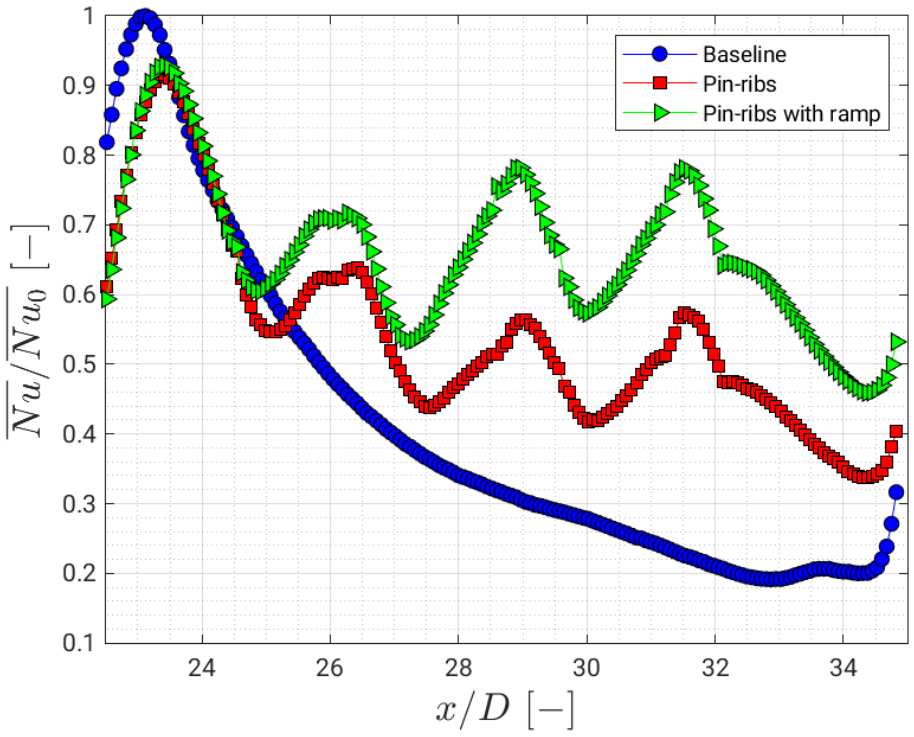

Figure 31: *Spanwise-averaged data of Figure 30 with focus on the last impingement jet and the transition zone.*

4.1.9 Summary of main findings

The heat transfer test results have shown that the Nu values in the impingement area are similar for both channels, and that this is not affected by the addition of enhancement features in the transition zone, with some exceptions:

- When the enhancement feature is placed close to the last impingement jet, the Nu distribution and the maximum value in the stagnation zone are impacted.
- If a bypass between the 1st and 2nd channel is present, the Nu distribution in the 2nd channel is strongly modified, with lower average Nu.

Increasing the number of jets in the 1st channel slightly increases the heat transfer in the transition zone thanks to the higher jet velocity. The increase in the covered area and total mass flow, however, does not allow a direct comparison. The same holds true for different transition lengths, where the average Nu cannot be directly compared due to the different sizes of the covered area.

The addition of turbulence enhancing features like ribs, pins, or cross-section reduction increases the average heat transfer in the transition zone. Combining these features brings even more improvement. However, combining these features translates directly to a smaller passage area for the flow in the transition zone. For this reason, a fair evaluation of the performances needs to also compare the pressure losses through the complete channel and the used massflow.

4.2 Pressure losses

The experimental models are instrumented with several pressure taps to gather information about the pressure losses of each component of the cooling channel (see also Figure 4). In particular, we are interested in the total pressure losses, which can be broken down in 3 components:

- the losses associated with the air flowing through the impingement holes in the first channel,
- the losses associated with the flow in the transition zone and through the purge hole,
- the losses associated with the air flowing through the impingement holes in the first channel.

To get an idea of the losses associated with each component, Figure 32 shows the pressure loss through the complete channel, as well as the breakdown for each component, as a function of Reynolds number for the baseline configuration. The flow through the 1st and 2nd impingement holes are the main contributors of the losses, with the losses in the 2nd channel being slightly higher than the 1st; this can be attributed to the different flow configuration in the 2nd plenum. The flow through the purge hole accounts for roughly half of the losses compared to the impingement channel. This makes sense, since the purge hole area is double that of the impingement holes.

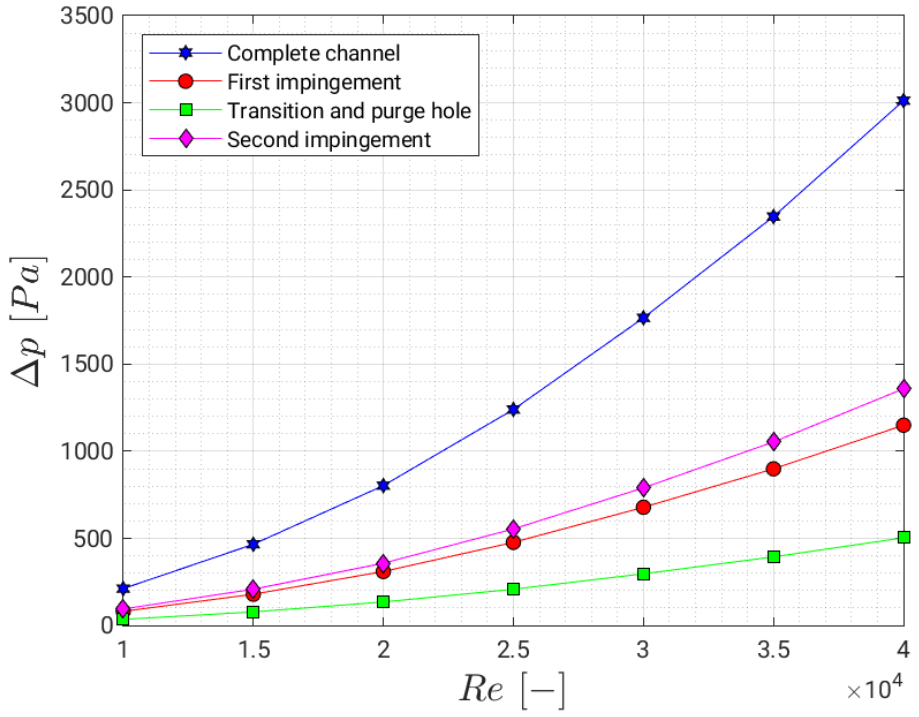

Figure 32: *Pressure losses of the baseline channel (5510) and contribution of each channel segment as a function of Reynolds number.*

More relevant information on the magnitude of the losses can be obtained by computing the so called discharge coefficient, which is the ratio of the actual massflow through a hole to the massflow one would get with a perfect nozzle with the same throat area isentropically expanding a fluid between the same pressures. It can be computed with the following formula:

$$C_d = \frac{\dot{m}}{A\sqrt{2\rho\Delta p}}$$

Where $\dot{m}$ and Δp are the measured massflow and pressure loss, respectively, ρ is the density and A is the hole area considered (i.e. the total area of the impingement holes of the channel when considering the impingement area, and the purge hole area when considering the flow through the purge hole).

In essence, the discharge coefficient is 1 if the flow has no losses and tends to 0 when the losses increase.

All configurations have a discharge coefficient of ~0.85 for the 1st and 2nd impingement, with the exception of the 2nd channel of the bypass cases, where the computation of the discharge is not strictly correct, since the actual massflow going through the impingement holes is lower than the total massflow for the 2nd channel. The value of 0.85 is higher (i.e. the losses are lower) than commonly assumed for round nozzles (a value around 0.75 is usually measured). The higher value is attributed to the fact that the impingement holes are chamfered on both sides. This fact has been checked by measuring the pressure losses of one of the channels used in a previous project, which had a sharp-edged hole, obtaining a value of 0.76, and then by measuring the same channel but with chamfered holes, obtaining 0.86, consistent with the findings in the present work.

Regarding the losses of the transition zone and purge hole, the discharge coefficient for the baseline configuration is around 0.63, and the losses are mainly associated with the purge hole, since the flow past the smooth transition zone does not incur significant losses.

4.2.1 Purge hole discharge factor of all configurations

Since the losses of the impingement flow are largely independent from the enhancement features present in the transition zone, the pressure loss comparison should focus on the transition zone and purge hole losses. Figure 33 shows the discharge factor as a function of the area-averaged Reynolds number. Configurations with a small open area, for instance ribs with a big ramp or pin-ribs and small ramp, tend to have low discharge coefficients (high losses). To improve the losses compared to the baseline, the transition zone needs to be reduced or a bypass introduced. Another possibility of reducing the losses is by using the short version of the ramp, which has a rounded corner upstream of the purge hole that helps to keep the discharge flow attached. This is particularly evident for the small ramp case (5510RS). It has to be noted that the small, short ramp can be combined with the ribs to achieve lower losses than the baseline (although not as good as the ramp alone) and higher heat transfer (see configurations 5510DVRR, 5510DCRR).

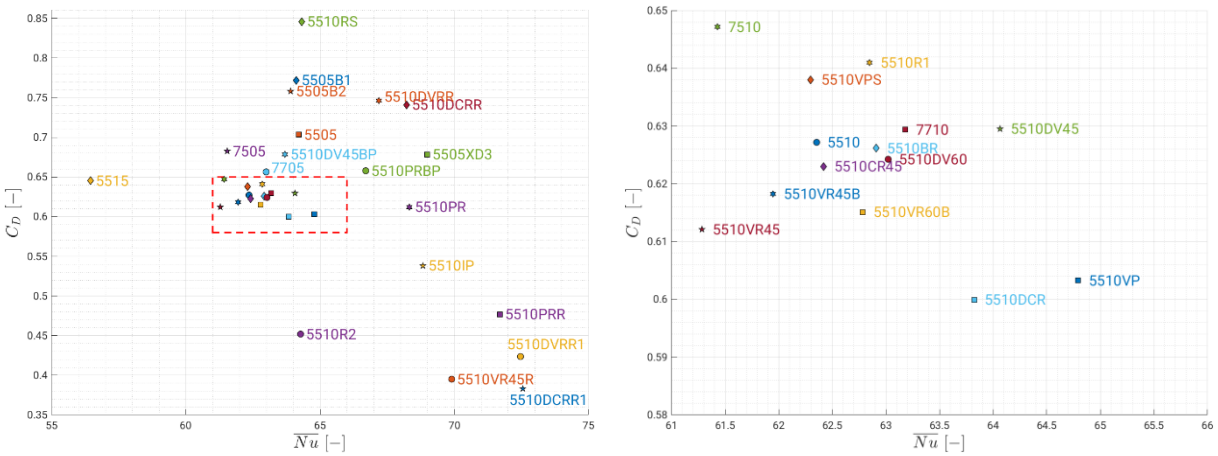

Figure 33: Discharge factor through the purge hole as a function of the area-averaged Nusselt number in the 1st channel. The right plot is a zoom into the central part of the left plot. Values are the average over the Reynolds numbers tested (10000, 20000, 40000).

4.3 Multi-objective evaluation of the geometries

Figure 33 used the area-averaged Nu as a performance parameter for the heat transfer. However, such a comparison between configurations is not necessarily consistent for two reasons:

- the configurations can have different target surfaces.
- the total massflow for the same Reynolds number varies according to the number of jets in the 1st channel.

To have a better figure of the thermal performance of each configuration, the above 2 points must be included in the area-averaged Nusselt number analysis. In order to do this, the Nusselt number is multiplied by the target area of the 1st channel, to favour configurations that cool a bigger surface, and divided by the total jet hole area of the 1st channel (which is directly proportional to the total massflow) to favour configurations using less cooling air. Figure 34 shows this modification. Here, better solutions are located towards the upper right corner of the graph.

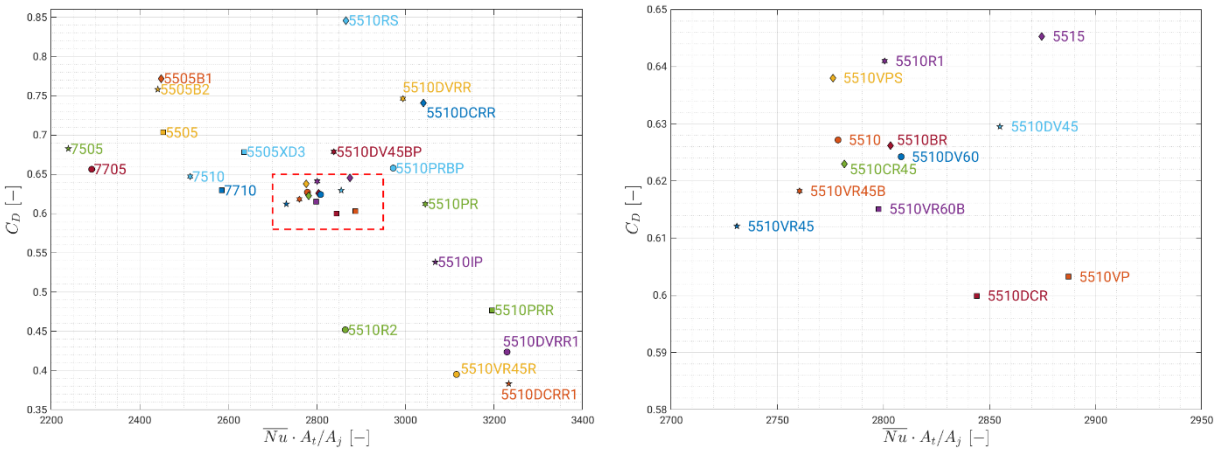

Figure 34: *Discharge factor through the purge hole as a function of the area-averaged Nusselt number in the 1st channel multiplied by the ratio of target area to jet area. The right plot is a zoom into the central part of the left plot. Values are the average over the Reynolds numbers tested (10000, 20000, 40000).*

Additionally, since the transition zone is the most critical part of the channel, experiencing the highest temperature in operation (see next section), to evaluate the optimal configurations in a more relevant way, one could restrict the heat transfer analysis to the transition zone. Figure 35 shows the same analysis as Figure 34 but the area-averaged Nu is restricted to the transition zone. Again, optimal geometries are on the upper right corner of the graph. There are 9 geometries that are optimal in a Pareto sense (i.e. geometries for which a better solution for both objectives cannot be found).

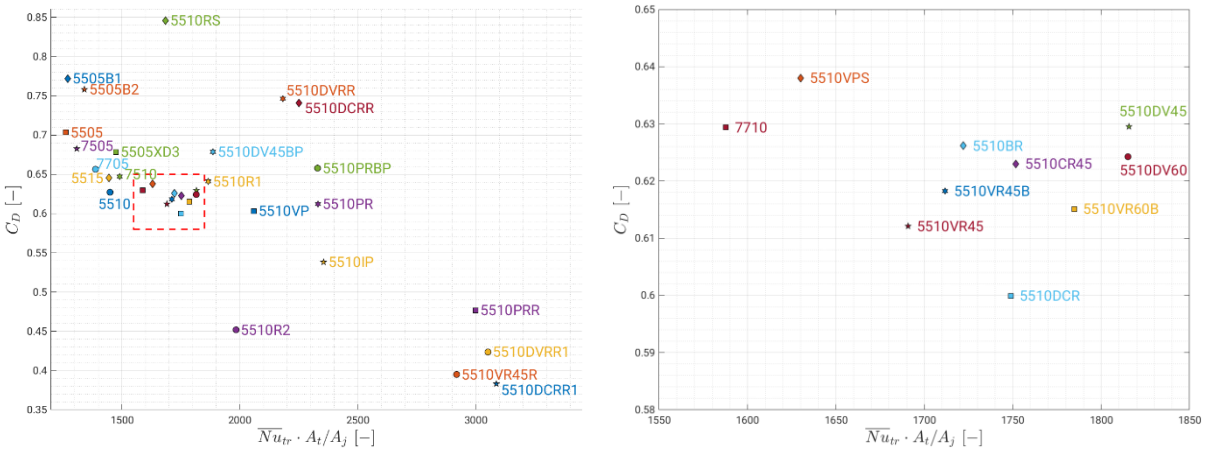

Figure 35: *Discharge factor through the purge hole as a function of the area-averaged Nusselt number in the transition zone multiplied by the ratio of target area to jet area. The right plot is a zoom into the central part of the left plot. Values are the average over the Reynolds numbers tested (10000, 20000, 40000).*

The optimal geometries, listed from the one with the lowest pressure losses to the one with the maximum Nu are:

- 5510RS: small ramp
- 5510DVRR: discrete V-ribs and small ramp
- 5510DCRR: discrete chevron ribs and small ramp
- 5510PRBP: pin-ribs with bypass
- 5510PR: pin-ribs
- 5510IP: inclined pins
- 5510PRR: pin-ribs with small ramp
- 5510DVRR: discrete V-ribs and big ramp
- 5510DCRR: discrete chevron ribs and big ramp

These optimal configurations can be clustered in three groups based on their heat transfer characteristics:

- Cluster 1: 5510RS
- Cluster 2: 5510DVRR, 5510DCRR, 5510PRBP, 5510PR, 5510IP
- Cluster 3: 5510PRR, 5510DVRR, 5510DCRR

Furthermore, in each cluster a best candidate can be found by analysing the trade-offs between candidates:

- Cluster 1: only one candidate, **5510RS**
- Cluster 2: **5510DCRR**. Slightly higher losses than 5510DVRR but higher heat transfer. Much lower losses than other candidates with similar heat transfer.
- Cluster 3: **5510PRR**. Slightly lower heat transfer than other candidates but much lower losses.

The final choice is case specific and depends on the available pressure difference to drive the flow, since the spent cooling air is generally injected in the hot flow for film cooling. These 3 configurations, along with the baseline, are further analysed in terms of performances in a real world scenario in the next section.

4.4 Analysis of selected solutions in a real-case scenario

4.4.1 Comparison with a single impingement channel

To assess the performance of the sequential impingement channels, the evolution of the coolant and the target plate temperature along the channel are derived with a simplified analytical approach, and the results compared to a single impingement channel of the same length.

We consider a single impingement channel with 12 holes and same jet-to-jet spacing and channel cross-section as the baseline channel analysed in this project. By using 12 holes, the single impingement channel has the same length as the baseline sequential channel, so that the cooled surface is the same in both cases.

The coolant mass flow is considered the same in both channels. Since no tests have been performed in-house on a 12 holes channel, data from the literature are used [9], which refer to a channel of a single row of 15 narrow impingement channels, the main difference being that the width of the channel is 4D instead of 5D in the present study. The results, however, compare well with the present study when normalized by the Reynolds number (Figure 36) for the first five jets: the discrepancy of the minima may be attributed to the different channel width, and the discrepancy of the maxima for jet number 4 and 5 to the different crossflow velocity. The cause for the discrepancy of the first maximum is unclear, but it has to be noted that the spacing between the first jet and the upstream wall seems to be 5.5 jet diameters in the referenced study, while it is 2.5 jet diameters in the present study. Nevertheless, the area-averaged Nu for the first five holes is very similar between the two studies: $Nu/Re^{0.7}$=0.063 for the single channel, $Nu/Re^{0.7}$=0.067 for the sequential channel.

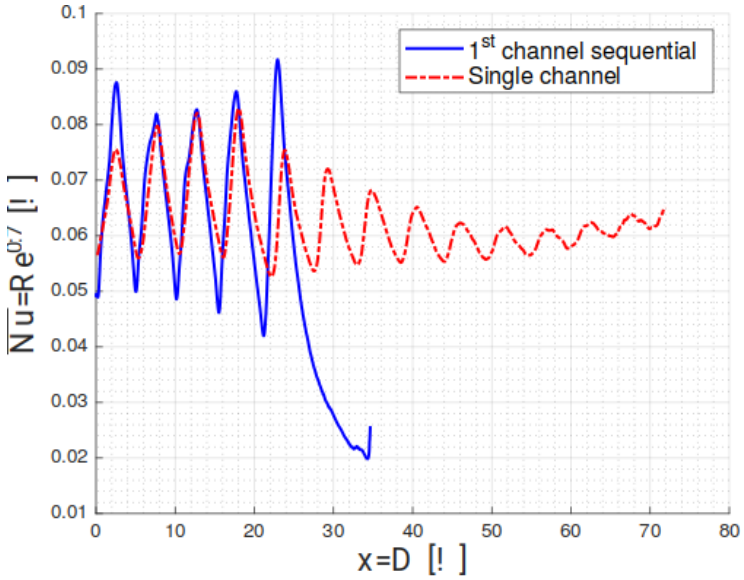

Figure 36: *Spanwise-averaged normalized Nusselt number for the first channel of the sequential impingement (blue) at Re=40000 and a single channel with 15 holes at Re=30000 (red, data extracted from [9]).*

We consider a metallic target plate of length 60D and width 5D subjected, on the external side, to typical engine level conditions assumed from [10]: a flow at temperature T_{ext} and with a heat transfer coefficient h_{ext}=1135 W/m^2 K, assumed constant along the blade, while on the internal side, the plate is cooled by impinging jets with a jet temperature T_0. The jet diameter considered is D=1.5 mm. The objective is to determine the coolant and plate temperature along the channel for the single and sequential impingement channels, respectively.

To find the temperature distribution along the channel, the problem is divided into 12 stations (one for each jet).

For the single impingement channel, the metal temperature is found by equating the external heat transfer to the internal heat transfer:

$$h_{ext}(T_{ext} - T_M) = \bar{\bar{h}}(T_M - T_{cooling})$$

where $\bar{\bar{h}}$ is the average heat transfer coefficient for the station considered, obtained by averaging the data from Fig. 6 and using the jet Reynolds number of the channel considered (Re=40000 for the sequential channel, and Re=16670 for the single channel). Additionally, $T_{cooling}$ is the mass-averaged temperature of the jet flow at the station considered and the spent air (crossflow) from the previous stations, which is at higher temperature due to the picked up heat.

The temperature increase of the coolant can be found by equating the heat pickup of the coolant and the heat transfer:

$$\dot{m}c_p\Delta T = h_{ext}(T_{ext} - T_M)S$$

where $\dot{m}$ is the sum of the massflow of the jet and the crossflow at the station considered. Here it is assumed that the total massflow is distributed equally between the jets, and that the initial temperature of the flow at that station is the massflow-averaged sum of the jet temperature, at T_0, and the crossflow, at higher temperature due to the cooling action performed at the previous stations.

For the sequential channel, the same procedure is applied, with the difference that in the transition zone (stations 6 and 7), there are no jets, so there is no addition of “fresh” air and no increase in the mass flow. A jet Reynolds number Re=40000 is considered for the sequential impingement channel. To keep the total massflow constant, the jet Reynolds number in the single channel must be reduced to Re=16,670; the available data being at Re=30000, Nusselt number data are scaled with Re$^{0.7}$.

In Figure 37, the metal and coolant temperature evolution along the channel for a single and sequential impingement at the same coolant massflow are shown in non-dimensional form, obtained with the following formula:

$$T^* = \frac{T - T_0}{T_{ext} - T_0}$$

Thanks to the higher jet Reynolds number, the sequential impingement achieves lower metal temperatures in the impingement area of both channels (stations 1-5 and 8-12), but the low heat transfer in the transition zone causes a high metal temperature in that region (see stations 7-8), as well as strong temperature gradients, that can cause excessive thermal stresses in the blade. Moreover, the cooling fluid is more efficiently used, as can be deduced from the higher coolant outlet temperature (station 12).

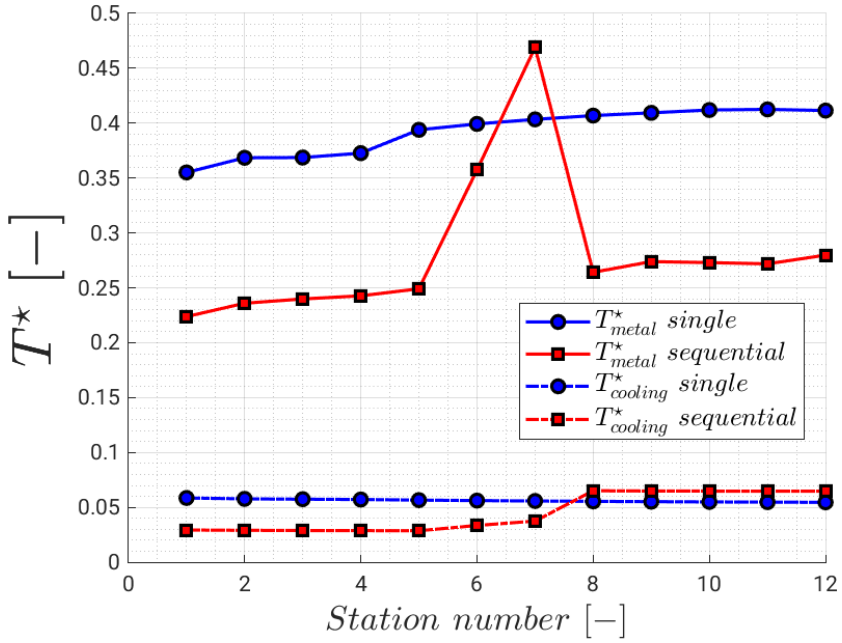

Figure 37: *Cooling air and non-dimensional metal temperature for a single and a sequential impingement channel at the same total mass flow. Jet Reynolds number is Re=40000 for the sequential channel and Re=16670 for the single channel.*

If the same analysis is performed for the 3 optimal configurations identified in the previous section, the metal temperature in the transition zone can be strongly reduced (Figure 38). Of course this reduction goes hand in hand with an increase of the pressure losses, with the exception of the small ramp case (green line) that achieves lower losses than the baseline.

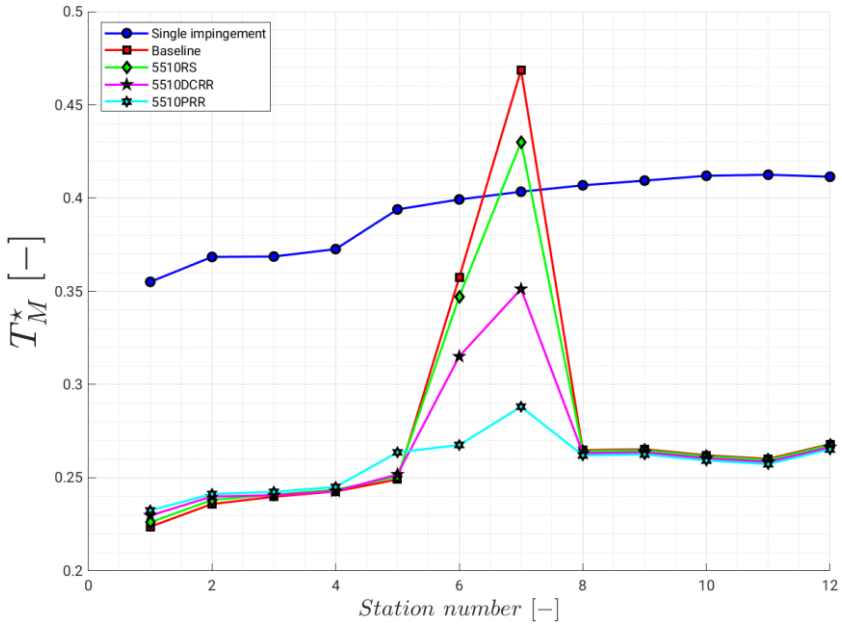

Figure 38: *Non-dimensional metal temperature for a single and the optimal sequential impingement channels at the same total mass flow. Jet Reynolds number is Re=40000 for the sequential channels and Re=16670 for the single channel.*

4.4.2 Analysis of a complete turbine cycle

To assess the potential of the sequential impingement solution, the approach of the previous section is integrated into a complete cycle of a gas turbine. A generic turbine cycle is considered, loosely based on ANSALDO GT26 gas turbine, a 300MW advanced class gas turbine. This turbine features a so-called sequential combustion strategy, where the first combustion chamber has a very lean mixture, after which the flow is expanded in the high pressure turbine and re-heated in a second combustion chamber. This arrangement is chosen here since it has been recently shown that such a machine can burn mixtures of hydrogen and natural gas, or even pure hydrogen, with only minor modifications [4].

A representative enthalpy-entropy (*h*-*s*) diagram for the cycle is shown in Figure 39. The flow is compressed from 1 to 2, the first combustion chamber brings the flow to the point 3HP, followed by the high pressure turbine (3HP to 4HP), re-heat in a second combustion chamber (4HP to 3LP) and finally the low pressure turbine (3LP to 4LP). To compute the cycle, the following assumptions are made:

- Isentropic losses of 10% in the compressor and 8% in the turbines. Pressure losses in the combustion chamber 5%.
- Total massflow 650 Kg/s
- Turbine entry temperature (TET) 1700 K for both turbines.
- Overall pressure ratio: 34 bar
- 12% of the massflow is used for cooling, using a single impingement cooling solution, split equally between the 1st stages of the HP and LP turbine.

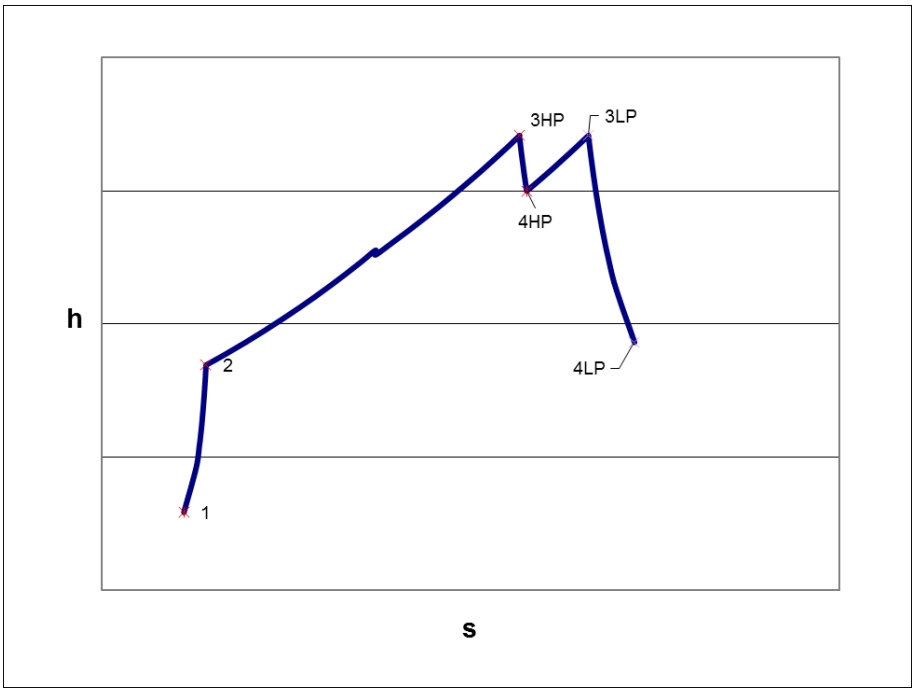

Figure 39: *Thermodynamic cycle of a gas turbine with sequential combustion.*

The idea is to compute the cycle of this machine, to find its thermal efficiency, and then recompute the cycle by considering the optimal cooling methods identified above. The approach used in the previous section is used to find the coolant massflow needed to reach the same TET as for the single impingement case.

If the thermal performances of the cooling channel are higher, less coolant is used. The difference can be used in the hot path. As a simplification, it is considered that the coolant used in the HP turbine does not contribute energy in the HP turbine, but does so in the LP turbine. The coolant used in the LP turbine, however, is supposed to not create work useful work at all.

To find the coolant massflow used, the same approach as in the previous section is used, but instead of fixing the massflow like before, the required massflow is determined so that the maximum metal temperature is the same as in the single impingement case, essentially by finding the jet Reynolds number so that the maximum value of the curves in Figure 38 is equal to the maximum of the blue curve.

With this approach, the following values for the total massflow are found:

- Baseline (5510): $\dot{m}_c = 16.57\%$
- Small ramp (5510RS): $\dot{m}_c = 13.33\%$
- Discrete chevron ribs with small ramp (5510DCRR): $\dot{m}_c = 8.47\%$
- Pin-ribs with small ramp (5510PRR): $\dot{m}_c = 5.73\%$

The first 2 cases actually need more coolant than the single impingement case, since at constant massflow a higher metal temperature is obtained compared to the single impingement case (Figure 38). The discrete chevron ribs with small ramp and the pin-ribs with small ramp achieve a reduction of the coolant massflow, which translates in an increase of the thermal efficiency μ_{th}.

The above results assume that all actively cooled parts do so using impingement cooling. This is true for the heat shield and is a good assumption for the stator vanes (only the trailing edge is not cooled by impingement), but rotor blades are usually only cooled with impingement at the leading edge. We can thus assume that only 50% of the cooling air is used on the heat shield and stator vanes. To get a more realistic value of the coolant massflow used, the reduction of the coolant has to be cut in half, leading to these values:

- Discrete chevron ribs with small ramp (5510DCRR): $\dot{m}_c = 10.24\%$
- Pin-ribs with small ramp (5510PRR): $\dot{m}_c = 8.87\%$

By computing the thermodynamic cycle of the machine, one gets:

- Single impingement channel μ_{th}=42.18%
- Discrete chevron ribs with small ramp: μ_{th}=42.45%
- Pin-ribs with small ramp: μ_{th}=42.65%

So the improvement in efficiency for the best channels analysed in this project ranges from 0.64% to 1.11%.

To determine the potential savings in terms of CO_2 emissions, the following assumptions are made:

- Annual production of gas-fired plants: 5.9TWh (90% combined cycle, 10% single cycle)
- In combined cycle, 2/3 of the power is generated in the gas turbine
- Carbon content of the fuel: 49.24 Kg/MWh of chemical energy

Applied to the worldwide fleet of gas-fired power plants an improvement of the thermal efficiency of 1.1% represents a reduction of CO_2 emissions of 20000 Tons per year.

4.5 Experimental tests at full scale

Sequential impingement channels similar to the baseline geometry tested at EPFL have been integrated in the stator heat shield (SHS) of ANSALDO GT36 test gas turbine in Birr (AG). This test in a full scale gas turbine allows to validate the cooling concept in real conditions of pressure and temperature of both the hot flow coming from the combustion chamber and the coolant flow, and verify the results obtained in the lab at near ambient conditions. The surface in contact with the hot gas was instrumented with thermal paint, which enables the determination of the maximum temperature experienced at the surface during the test with great spatial resolution and low intrusiveness (see Figure 40). Results from the lab testing at EPFL have been integrated into the thermal modelling of this part and calibration of the numerical thermal simulations.

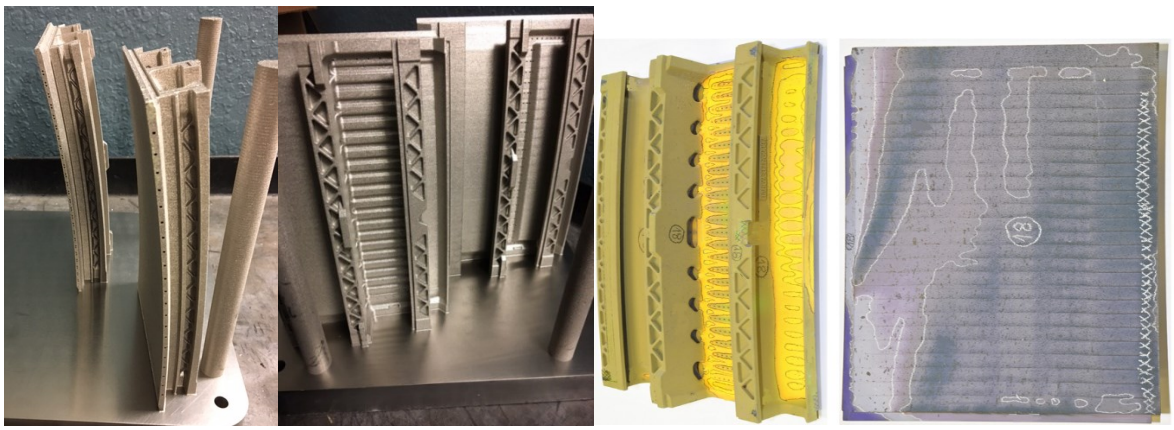

Figure 40: *Additively manufactured (SLM method) stator heat shield components before (left) and after (right) the thermal tests.*

The positive outcome of these tests allowed to proceed further and also integrate the cooling concept in more thorough testing, which included also other experimental parts [11]. The objectives of these tests were the following:

- Long duration tests to determine components lifetime and machine performance
- Short tests to check the behaviour during fast start-up and shut-down
- Long duration tests at off-design conditions for components lifetime and machine performance at off-design conditions (partial load).

The turbine section is instrumented with thermocouples, strain gauges, hot gas rakes, Kiel probes, pyrometers, static pressure taps, thermal paint, and 5-hole probes (see Figure 41). In total, the telemetry system receives data from more than 4000 instruments placed on all components of the machine and can test all operating conditions.

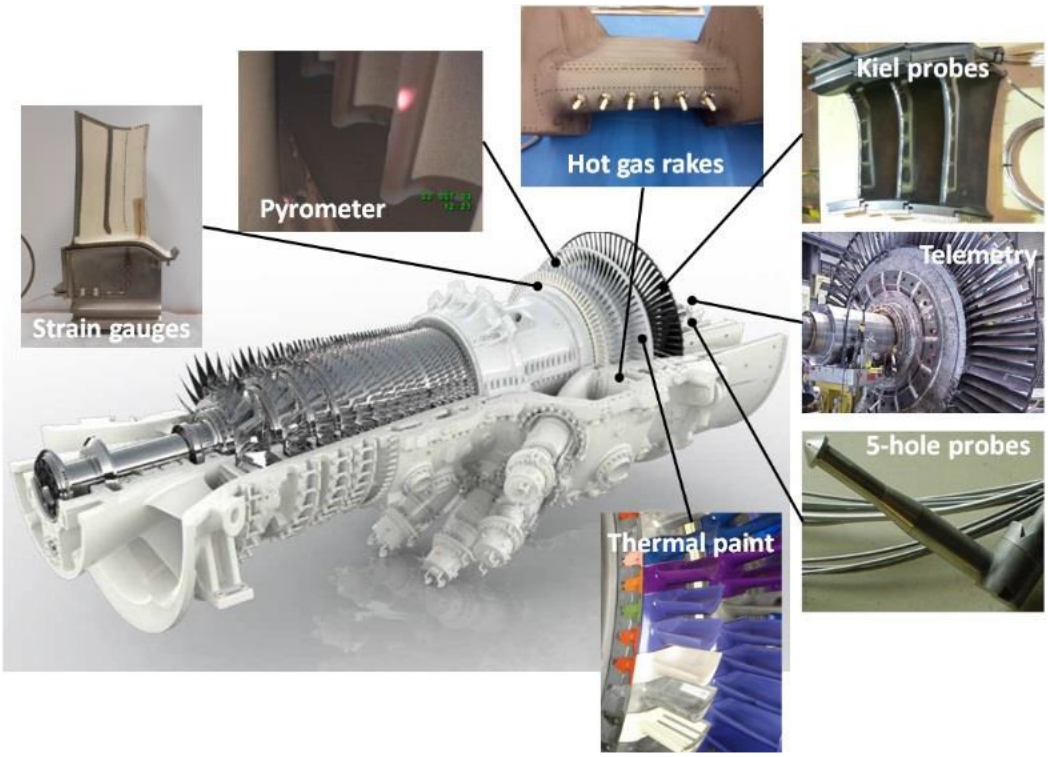

Figure 41: *GT36 test turbine and associated instrumentation.*

Figure 42 shows the time evolution of the surface temperature of turbine blades and vanes during a long duration test. The surface temperatures follow proportionally the hot gas temperature, and remain constant during steady operation, which indicates a highly responsive design of the internal cooling system.

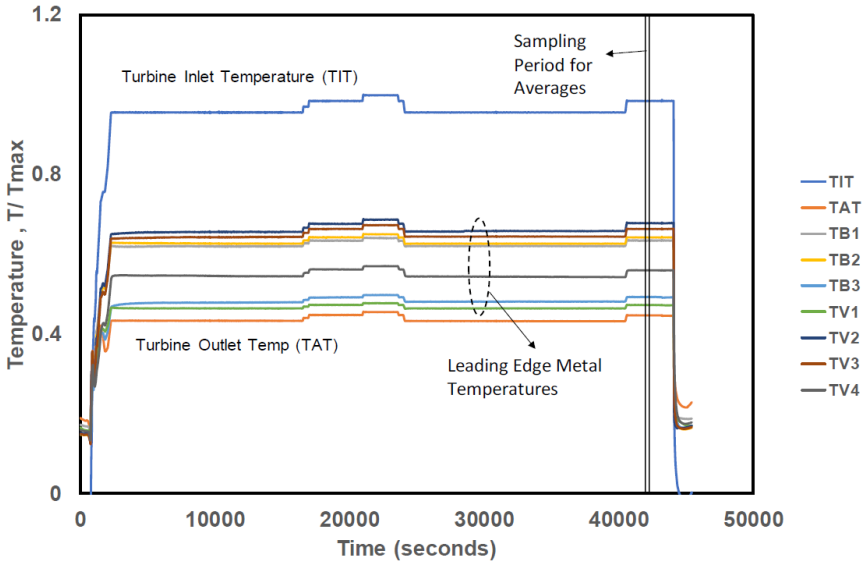

Figure 42: *temperature evolution on selected location of turbine blades and vanes during the long duration tests, as well as the hot gas flow inlet and outlet temperatures.*

For the short duration tests, the internal parts of the turbine (vanes, blades, heat shield) were coated with thermal paint (Figure 43), allowing the determination of the temperature distribution, and ultimately full validation of the thermal and cooling design of all the turbine components, by comparing the measured temperatures with the 3D numerical thermal models.

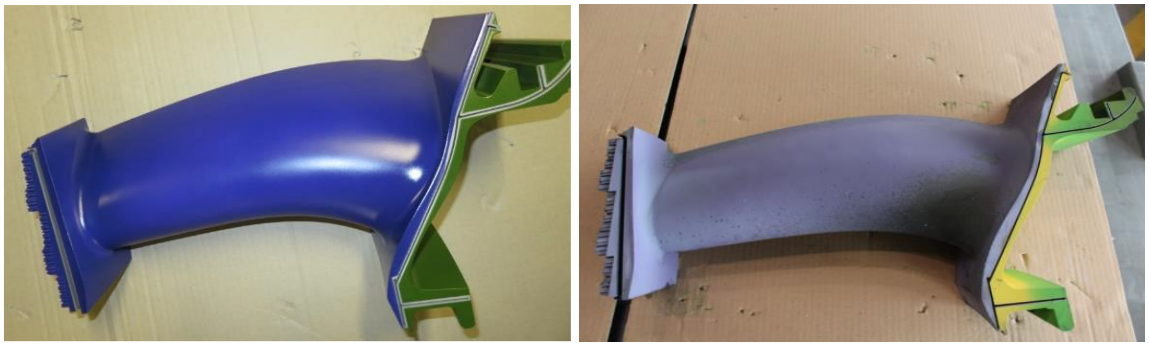

Figure 43: *turbine vane with thermal paint before (left) and after (right) the short duration tests.*

Full scale testing has allowed to bring the technology readiness level (TRL) of these novel cooling concepts to a value of 5-6. Parts have been tested at full scale in relevant conditions. In order to deploy this technology, further advancements have to be made in terms of manufacturing, life-cycle assessment, and maintenance.

5 Conclusions

In this project, several promising sequential impingement channel candidates for turbine cooling have been identified, and their performances evaluated. The geometrical variations of the channels concerned mainly the transition zone, which is a region with low heat transfer values. Heat transfer enhancing features, like pin-fins, ribs, and cross-section reductions help improve the heat transfer in this region, and allow the sequential impingement channels to achieve higher performances than state-of-the-art impingement channels.

In particular, a combination of discrete chevron ribs and a small cross-section reduction, as well as a combination of pin-ribs with a small cross-section reduction have been identified as optimal in terms of heat transfer and pressure losses, with the former geometry being better with respect to the pressure losses while the latter achieves better heat transfer. The choice of the optimal geometry in a real case scenario has to be done during the detailed design of the machine and would depend on the pressure difference available to drive the flow.

It has been evaluated that an efficiency improvement of up to 1.1% can be achieved by substituting a traditional narrow impingement channel with the optimal solution identified in the project. On a global scale, this would reduce the CO_2 emissions of currently operating gas fired plants by 20000 tons per year.

6 Outlook and next steps

Project results show that the novel solution for turbine cooling could lead to significant gains in the thermal efficiency of the machine. From a research point of view, shape optimization of the best solutions identified here could give an insight of the margin of improvement still available for this solution and to find a range of configurations that achieve different trade-offs between heat transfer capabilities and pressure losses, with the aim being to match the available pressure drop in each situation.

For all new technology introduction, Ansaldo Energia follows a Product Development Quality (PDQ) business process, which is an industry standard process and is common with all major gas turbine OEM's (Original Equipment Manufacturers). The PDQ quality process [12, 13], as shown below, addresses the full lifecycle of a new product introduction in a gas turbine power plant.

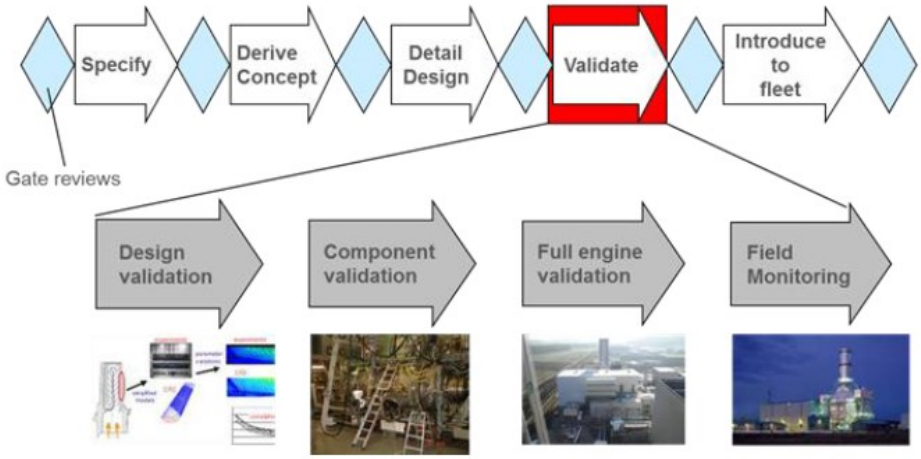

Figure 44: Ansaldo Energia Product Development Quality (PDQ) Business Process [9, 10].

The basic impingement cooling technology tested in the current EPFL research project is within the "Validate" phase of the PDQ business process and within the sub-process "Design Validation". The component and full engine validation phases shown above are described in [13]. In the full engine validation phase, the internal cooling system of one of the heat shield geometries tested at the EPFL laboratories was also tested [13]. The engine test results (thermal and mechanical) for this tested geometry generally confirmed predictions from the 3D finite element thermal and structural design models. The assumptions used in the 3D finite element thermal model with respect to the heat transfer coefficient and pressure drops were generally confirmed from the EPFL testing. Since several different geometries were tested in the EPFL test rig, the design space for the heat shield is extended and allows further optimization of the design.

As a next step for the market introduction of the advanced heat shield design, several important factors such as structural integrity, manufacturing and costs have also to be considered in the overall design of the component. Due to the high operating hot gas temperatures in gas turbines, the components are manufactured with very high grade metal alloys via specialized casting and machining operations. As this manufacturing process is cost intensive, it is planned that one of the optimized geometries tested at the EPFL will be manufactured and introduced within the next Ansaldo Energia gas turbine. This is expected to be within the next 1 to 2 years. With respect to the PDQ process, such a new technology introduction will then be continuously monitored in the field and further detailed

validation of the design will be performed to ensure that it fulfils the overall product specifications and costs.

7 National and international cooperation

The work has been carried out as a collaboration between the research partner, EPFL, and the industrial partner, ANSALDO Energia Switzerland, especially for the most important aspects of the project from an industrial point of view, which are the definitions of the geometries to be tested. In fact, it is important that the tested geometries can directly be applied to the cooling design for future gas turbine components, and that the acquired data are useful for expanding the cooling performance database and for the validation of numerical modelling tools that are used for the thermal design of the turbine. For this, regular contacts between the industrial partner and the academic partner have taken place during the project to define the test matrix and the details of the instrumentation of the test geometries. Tests have been organised in several campaigns, the last of which used configurations developed integrating the lessons learned on previous campaigns. Close collaborations between partners was needed to optimize these configurations.

Several project discussions have taken place to discuss the results during the project. The results from the EPFL test rig are very encouraging and are planned to be used in the design of future gas turbine components, which would further improve the performances of the sequential impingement cooling configurations.

During the entire duration of the project, ongoing work has been presented in international conferences related to gas turbines and to experimental techniques. Feedback from colleagues and experts has been valuable to improve both the experimental technique developed during the project and the geometries under study. The sequential impingement configurations have been met with positive interests at these venues.

8 Publications

Schmid, J., Gaffuri, M., Terzis, A., Ott, P., von Wolfersdorf, J. (2021), *Transient liquid crystal thermography using a time varying surface heat flux*, under review in: International Journal of Heat and Mass Transfer.

Gaffuri, M., Ott, P., Naik, S., Henze, M. (2021), *Heat Transfer Enhancement in a Double Sequential Impingement Channel*, ASME Turbo Expo 2021, virtual, online, June 7-11.

Gaffuri, M., Ott, P., Naik, S., Henze, M. (2021), *Experimental investigation of sequential narrow impingement channels for turbine cooling*, 14th European Confernce on Turbomachinery Fluid Dynamics & Thermodynamics, Gdansk, Pologne, April 12-16.

Schmid, J., Gaffuri, M., Terzis, A., Ott, P., von Wolfersdorf, J. (2020) *Accuracy Improvement of the Transient Heater Foil Technique for Heat Transfer Tests: Preliminary Results*. XXV Biannual Symposium on Measuring Techniques in Turbomachinery, Santorini, GR, September 21-23.

Gaffuri, M., Terzis, A., Ott, P. (2019), *Narrow Impingement Channels: Recent Advancements and Future Directions*, 14th European Confernce on Turbomachinery Fluid Dynamics & Thermodynamics, Lausanne, CH, April 8-12.

Gaffuri, M., Terzis, A., Ott, P., Retzko, S., Henze, M. (2018) *Evaluation of Heat Transfer Coefficients for an Impingement Cooling Cascade: Experimental Challenges and Preliminary Results*, XXIV Biannual Symposium on Measuring Techniques in Turbomachinery, Prague, CZE, August 29-31.

9 References

[1] Han, J. C., Dutta, S., & Ekkad, S. (2012). *Gas turbine heat transfer and cooling technology*. CRC press.

[2] Bunker, R. S., Dees, J. E., & Palafox, P. (2014). *Impingement Cooling in Gas Turbines: Design, Applications, and Limitations*. Impingement Jet Cooling in Gas Turbines, 25, 1.

[3] Llucià, S., Terzis, A., Ott, P., & Cochet, M. (2015). *Heat transfer characteristics of high crossflow impingement channels: Effect of number of holes*. Proceedings of the Institution of Mechanical Engineers, Part A: Journal of Power and Energy, 229(5), 560-568.

[4] Bothien, M. R., Ciani, A., Wood, J. P., & Fruechtel, G. (2019). *Toward decarbonized power generation with gas turbines by using sequential combustion for burning hydrogen*. Journal of Engineering for Gas Turbines and Power, 141(12).

[5] Terzis, A. (2014). *Detailed heat transfer distributions of narrow impingement channels for integrally cast turbine airfoils, PhD thesis n° 6177*. EPFL.

[6] Schmid, J., Gaffuri, M., Ott, P., & von Wolfersdorf, J. (2020) *Accuracy Improvement of the transient heater foil technique for heat transfer tests: Preliminary Results.* XXV Biannual Symposium on Measuring Techniques in Turbomachinery, Santorini, Greece.

[7] Llucià, S., Terzis, A., Ott, P., & Cochet, M. (2015). *Heat transfer characteristics of high crossflow impingement channels: Effect of number of holes.* Proceedings of the Institution of Mechanical Engineers, Part A: Journal of Power and Energy, 229(5), 560-568.

[8] Boonloi, A. (2014). *Effect of flow attack angle of v-ribs vortex generators in a square duct on flow structure, heat transfer, and performance improvement*. Modelling and Simulation in Engineering, 2014, p. 985612.

[9] Hossain, J., Tran, L. V., Kapat, J. S., Fernandez, E., and Kumar, R. (2014). *An experimental study of detailed flow and heat transfer analysis in a single row narrow impingement channel*. Turbo Expo: Power for Land, Sea, and Air, Vol. 45714, American Society of Mechanical Engineers, p. V05AT12A038.

[10] Lakshminarayana, B. (1995). *Fluid dynamics and heat transfer of turbomachinery*. John Wiley & Sons.

[11] Naik, S., Stephan, B., and Henze, M. (2021). *GT36 Turbine development and full-scale validation*, proceedings of ASME Turbo Expo 2021 Turbomachinery Technical Conference and Exposition, June 7-11, Virtual, Online.

[12] U. Ruedel, V. Stefanis, A. Ramaglia, S. Florjancic, *Development of the new Ansaldo Energia Gas Turbine Technology Generation*, Proc. of ASME Turbo Expo 2017, Charlotte, USA, GT2017-64893

[13] S.Naik, J.Krueckels, M.Henze, W. Hofmann. M. Schnieder, *GT36 Aero-thermal development and validation*, GT2017-64404, Proceedings of ASME Turbo Expo 2017, June 26-30, Charlotte, USA, 2017

Appendix 1: Heat transfer results in the 1st channel

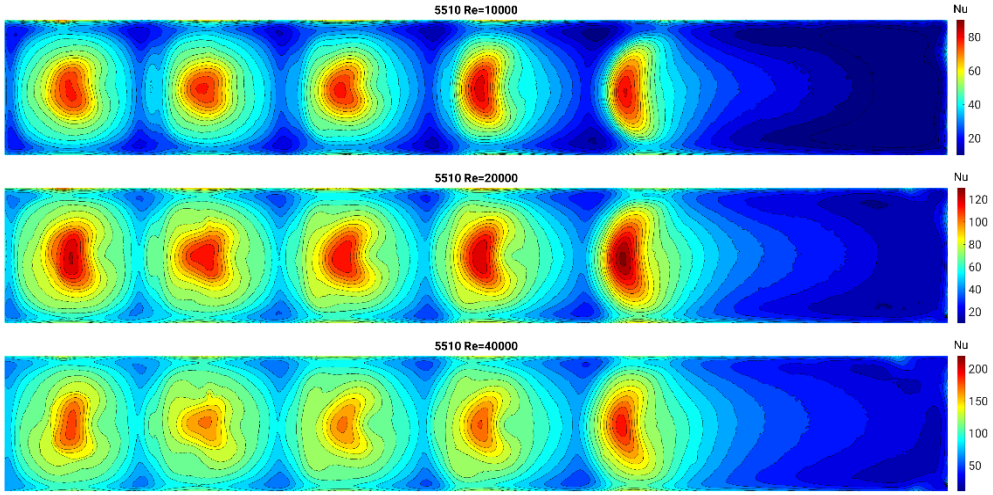

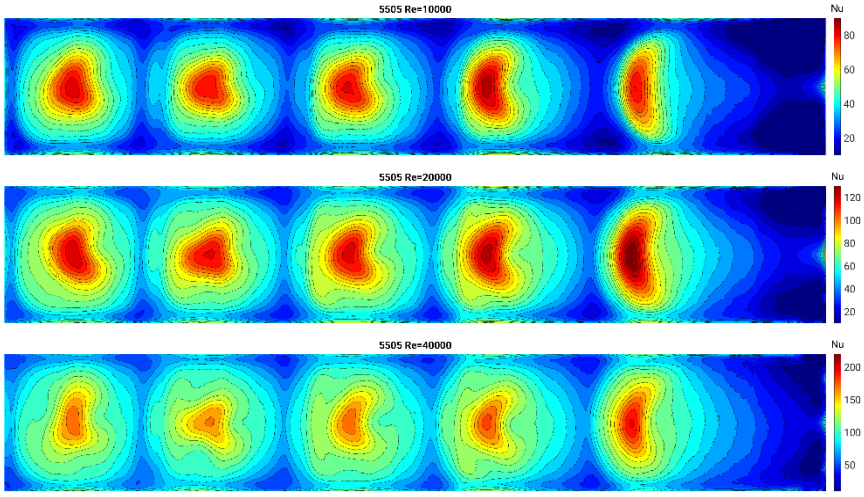

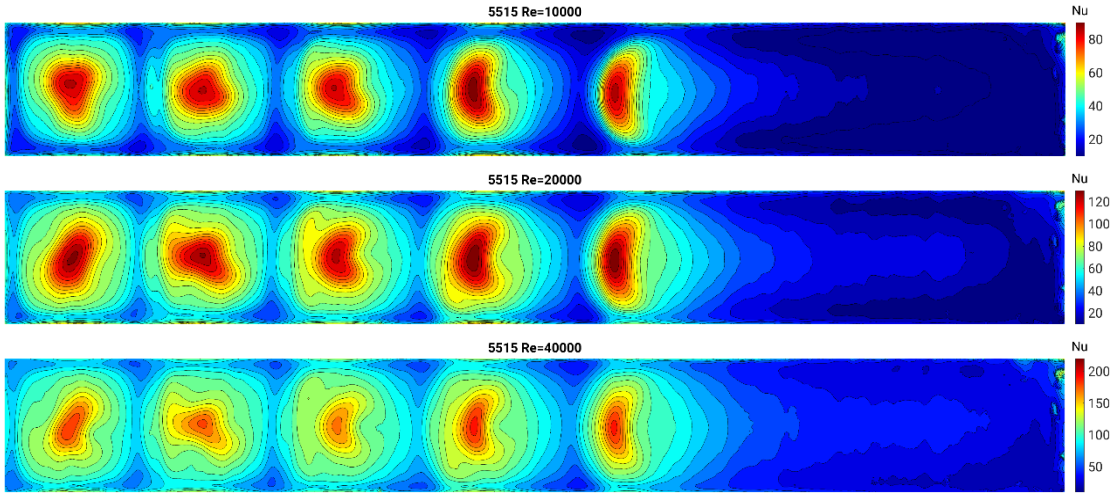

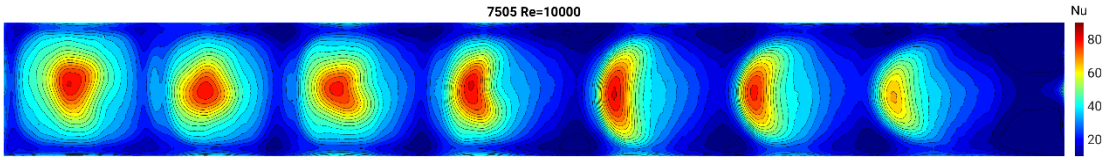
7505 Re=10000
Nu
80
60
40
20

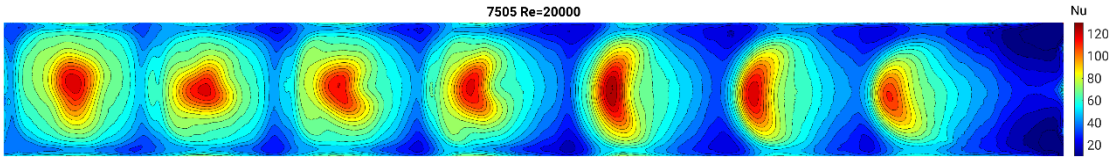
7505 Re=20000
Nu
120
100
80
60
40
20

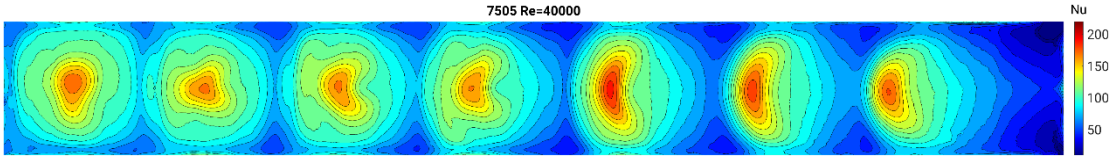
7505 Re=40000
Nu
200
150
100
50

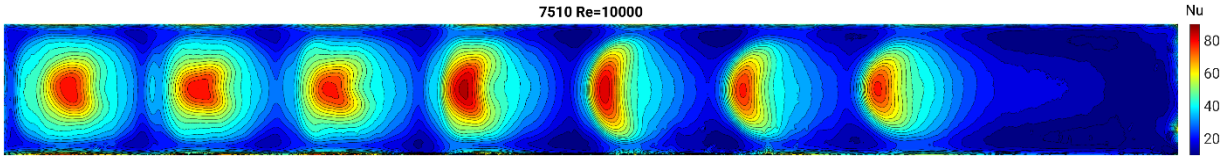
7510 Re=10000
Nu
80
60
40
20

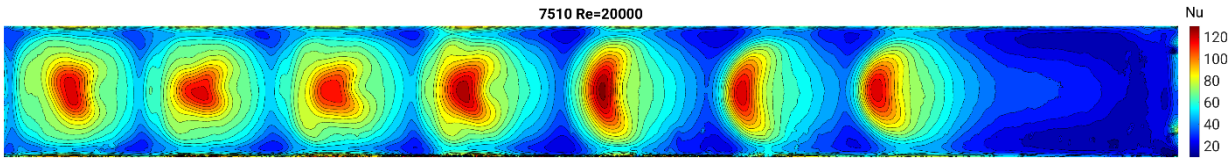
7510 Re=20000
Nu
120
100
80
60
40
20

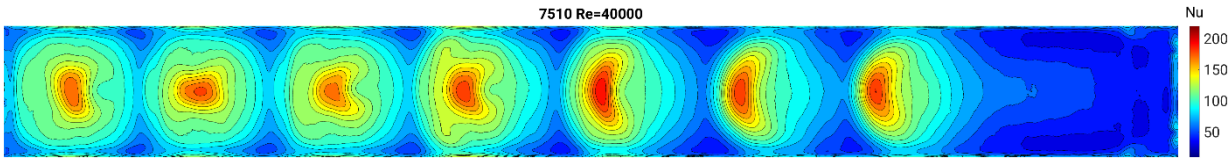
7510 Re=40000
Nu
200
150
100
50

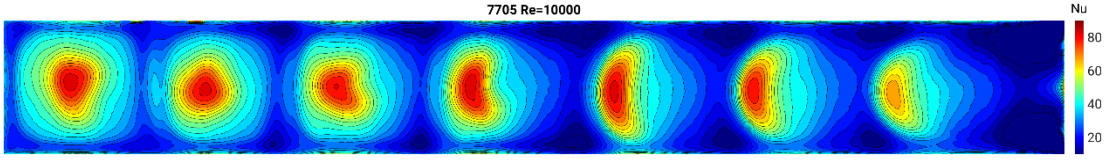
7705 Re=10000
Nu
80
60
40
20

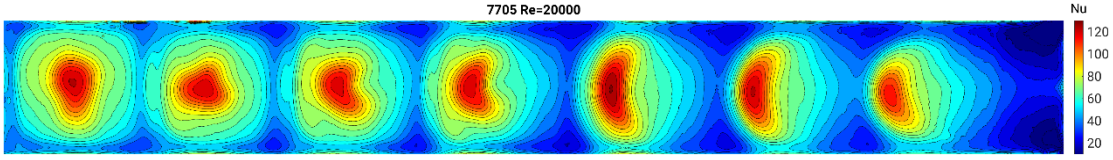
7705 Re=20000
Nu
120
100
80
60
40
20

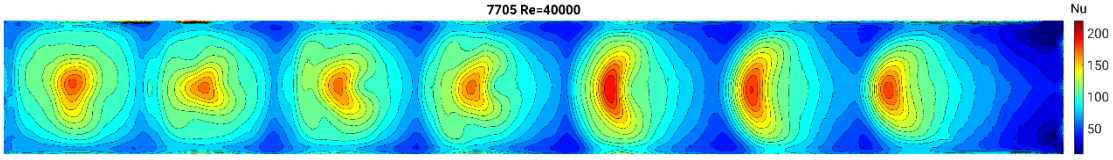
7705 Re=40000
Nu
200
150
100
50

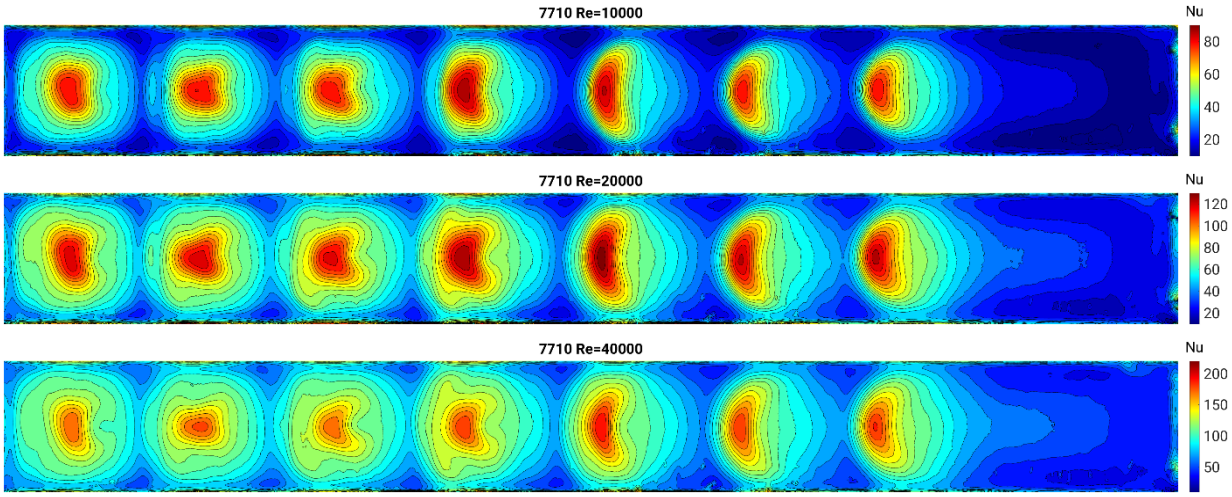
7710 Re=10000
Nu
80
60
40
20
7710 Re=20000
Nu
120
100
80
60
40
20
7710 Re=40000
Nu
200
150
100
50

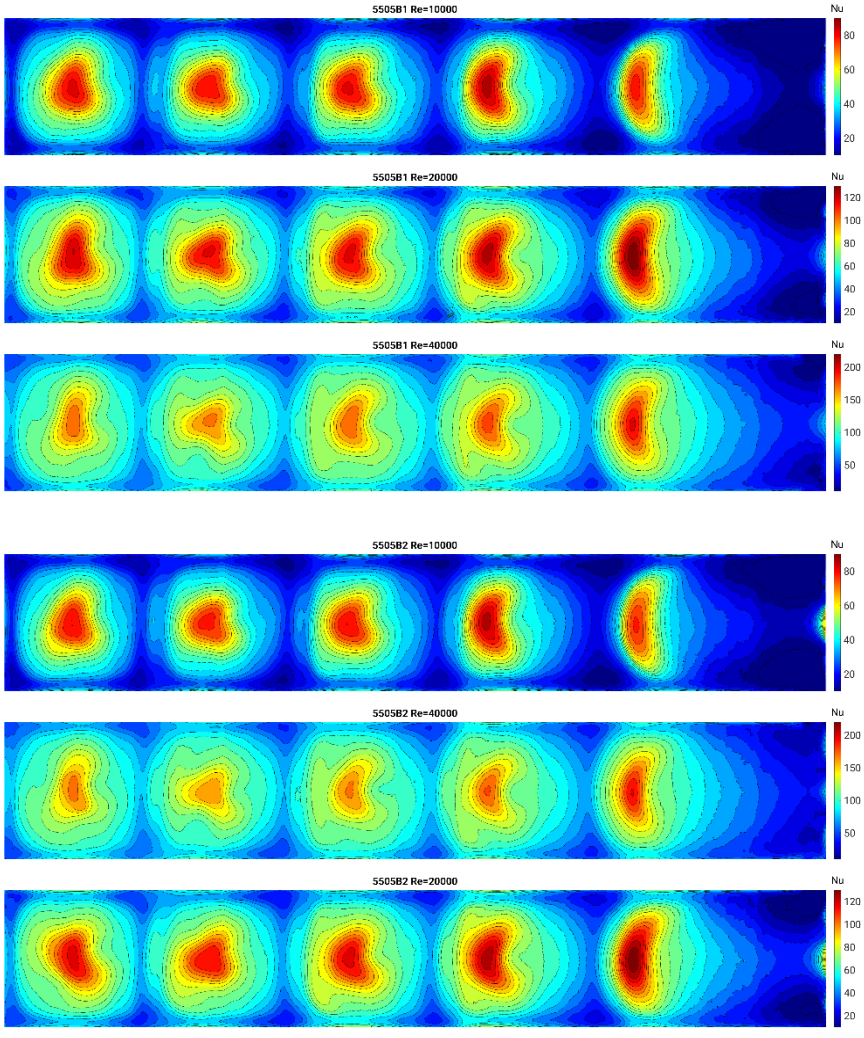
5505B1 Re=10000
Nu
80
60
40
20
5505B1 Re=20000
Nu
120
100
80
60
40
20
5505B1 Re=40000
Nu
200
150
100
50
5505B2 Re=10000
Nu
80
60
40
20
5505B2 Re=40000
Nu
200
150
100
50
5505B2 Re=20000
Nu
120
100
80
60
40
20

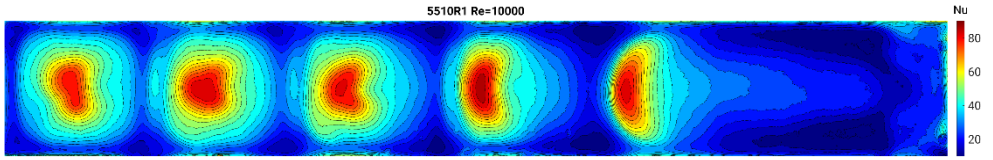
5510R1 Re=10000
Nu
80
60
40
20

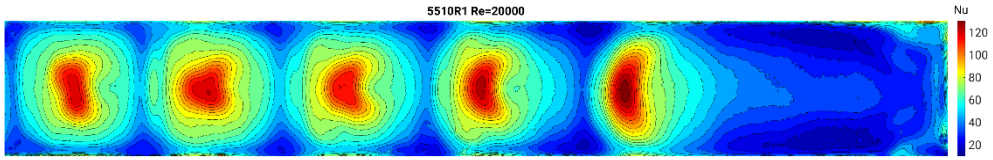
5510R1 Re=20000
Nu
120
100
80
60
40
20

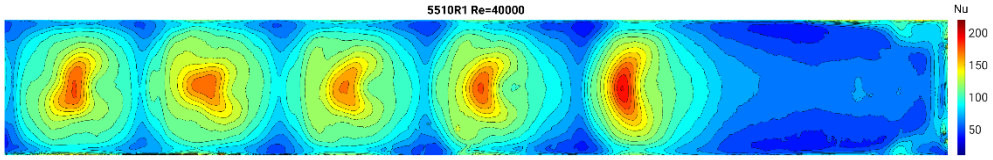
5510R1 Re=40000
Nu
200
150
100
50

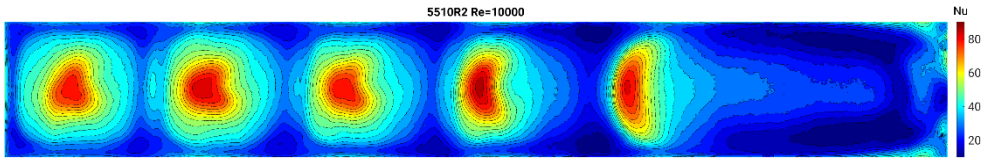
5510R2 Re=10000
Nu
80
60
40
20

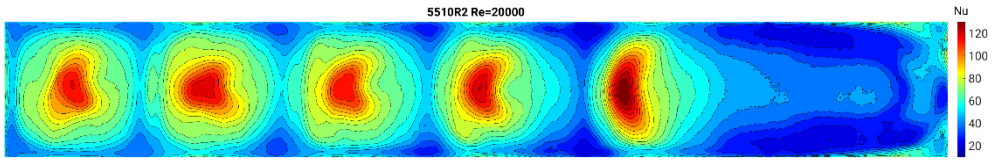
5510R2 Re=20000
Nu
120
100
80
60
40
20

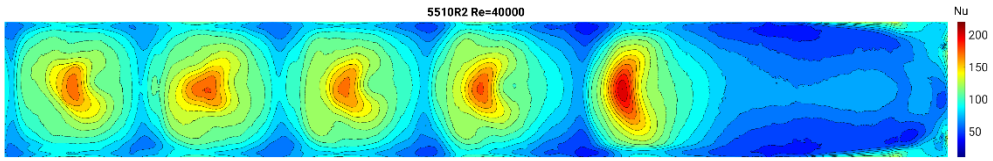
5510R2 Re=40000
Nu
200
150
100
50

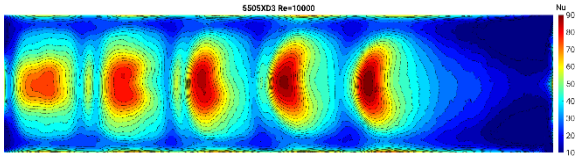
5505XD3 Re=10000
Nu

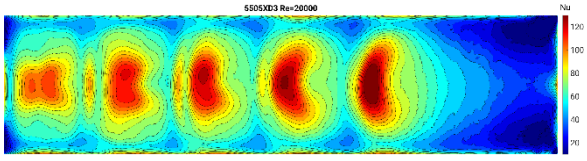
5505XD3 Re=20000
Nu

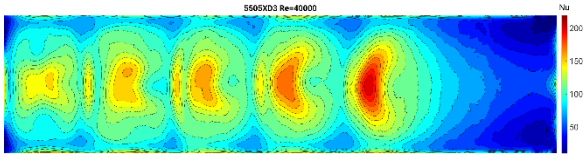
5505XD3 Re=40000
Nu

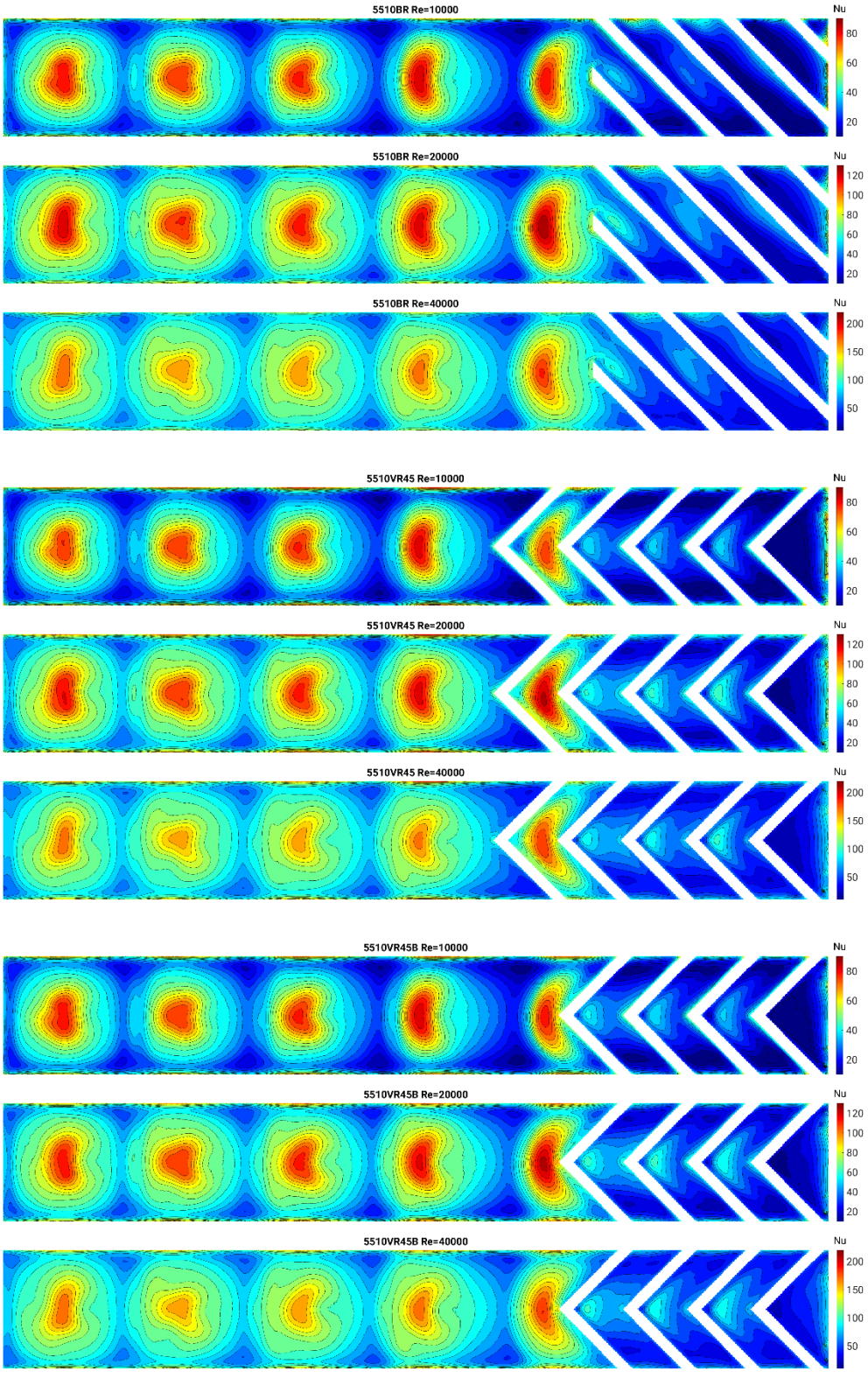
5510BR Re=10000
Nu
80
60
40
20
5510BR Re=20000
Nu
120
100
80
60
40
20
5510BR Re=40000
Nu
200
150
100
50
5510VR45 Re=10000
Nu
80
60
40
20
5510VR45 Re=20000
Nu
120
100
80
60
40
20
5510VR45 Re=40000
Nu
200
150
100
50
5510VR45B Re=10000
Nu
80
60
40
20
5510VR45B Re=20000
Nu
120
100
80
60
40
20
5510VR45B Re=40000
Nu
200
150
100
50

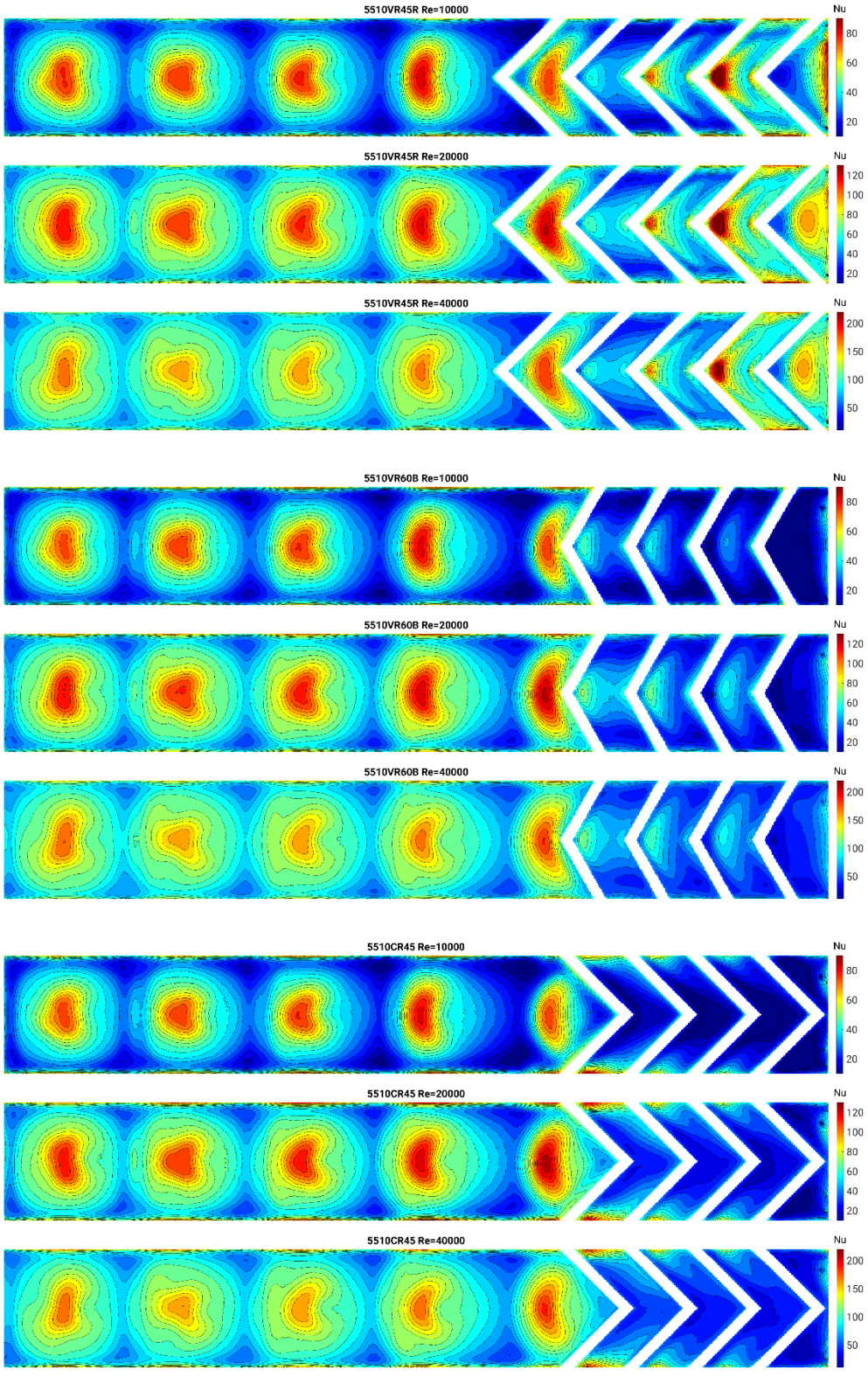
5510VR45R Re=10000
Nu
80
60
40
20
5510VR45R Re=20000
Nu
120
100
80
60
40
20
5510VR45R Re=40000
Nu
200
150
100
50
5510VR60B Re=10000
Nu
80
60
40
20
5510VR60B Re=20000
Nu
120
100
80
60
40
20
5510VR60B Re=40000
Nu
200
150
100
50
5510CR45 Re=10000
Nu
80
60
40
20
5510CR45 Re=20000
Nu
120
100
80
60
40
20
5510CR45 Re=40000
Nu
200
150
100
50

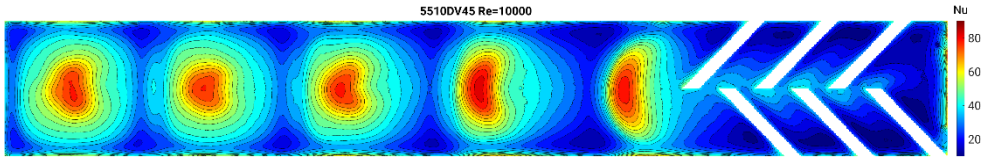
5510DV45 Re=10000
Nu
80
60
40
20

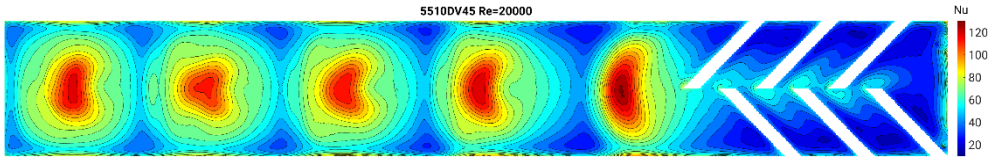
5510DV45 Re=20000
Nu
120
100
80
60
40
20

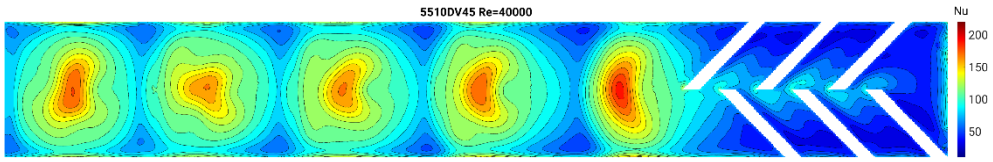
5510DV45 Re=40000
Nu
200
150
100
50

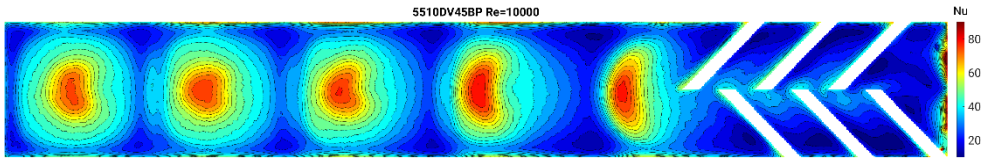
5510DV45BP Re=10000
Nu
80
60
40
20

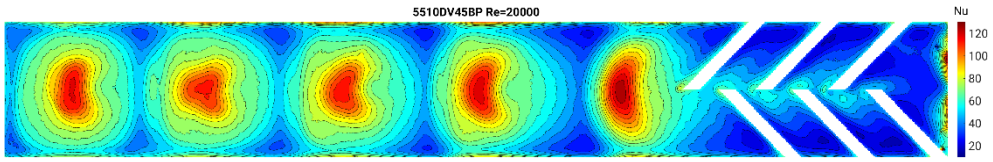
5510DV45BP Re=20000
Nu
120
100
80
60
40
20

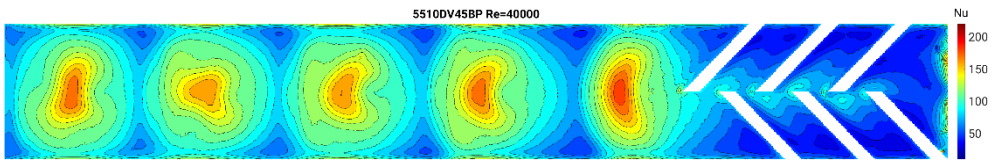
5510DV45BP Re=40000
Nu
200
150
100
50

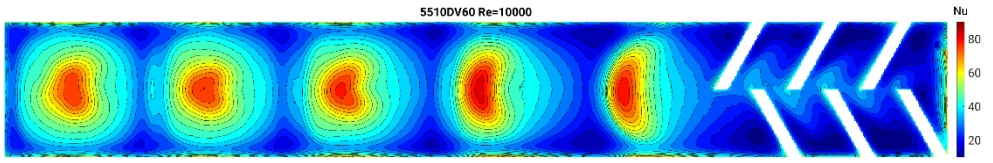
5510DV60 Re=10000
Nu
80
60
40
20

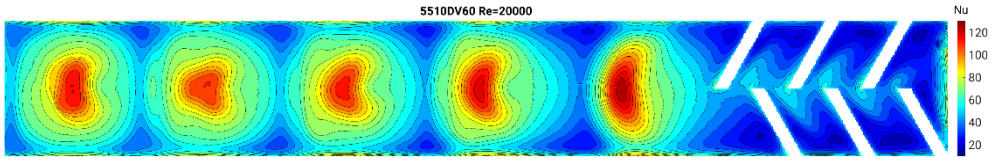
5510DV60 Re=20000
Nu
120
100
80
60
40
20

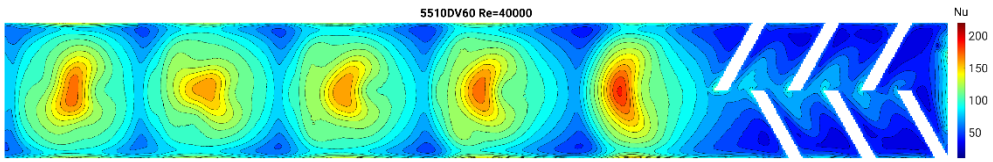
5510DV60 Re=40000
Nu
200
150
100
50

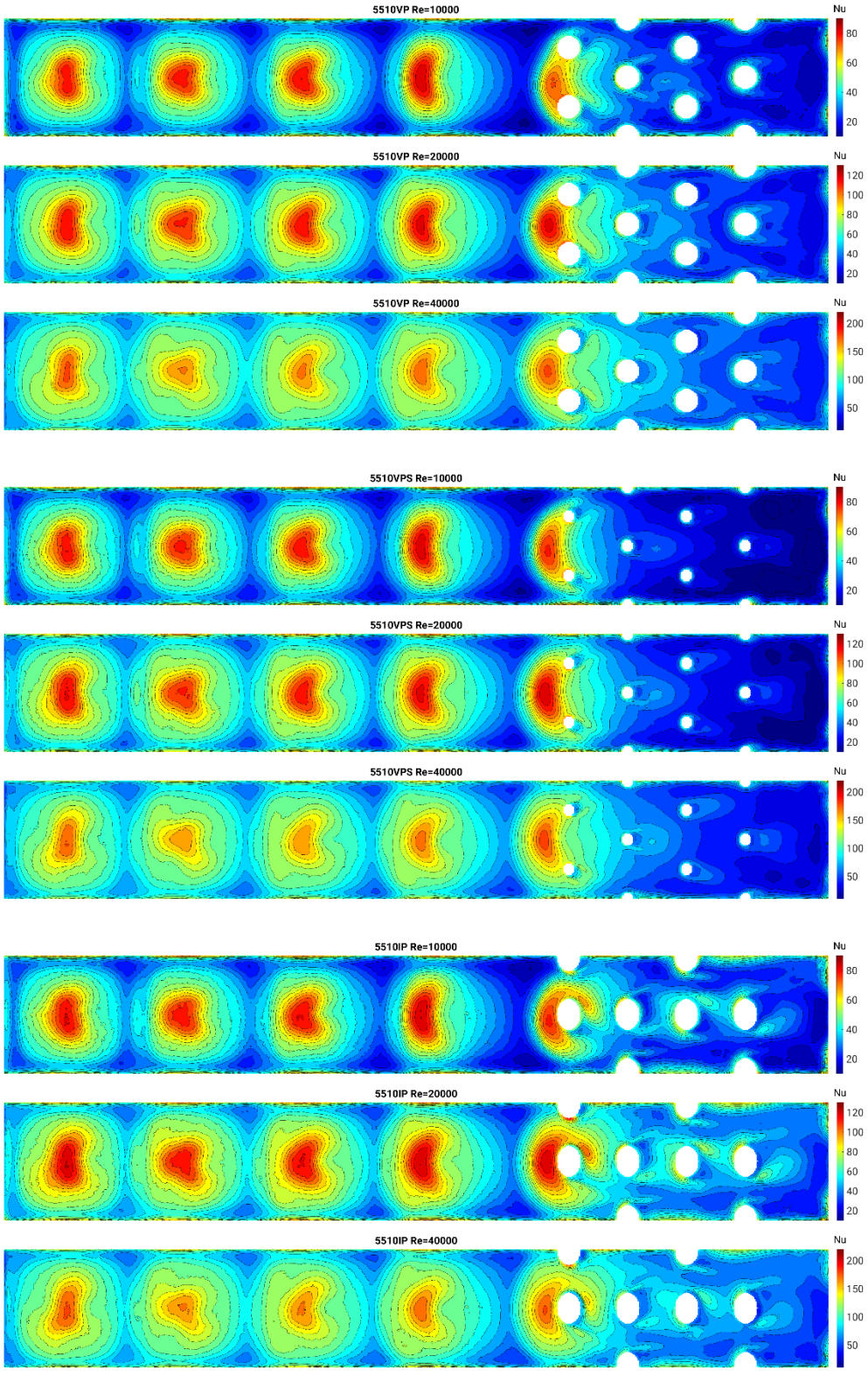
5510VP Re=10000
Nu
80
60
40
20
5510VP Re=20000
Nu
120
100
80
60
40
20
5510VP Re=40000
Nu
200
150
100
50
5510VPS Re=10000
Nu
80
60
40
20
5510VPS Re=20000
Nu
120
100
80
60
40
20
5510VPS Re=40000
Nu
200
150
100
50
5510IP Re=10000
Nu
80
60
40
20
5510IP Re=20000
Nu
120
100
80
60
40
20
5510IP Re=40000
Nu
200
150
100
50

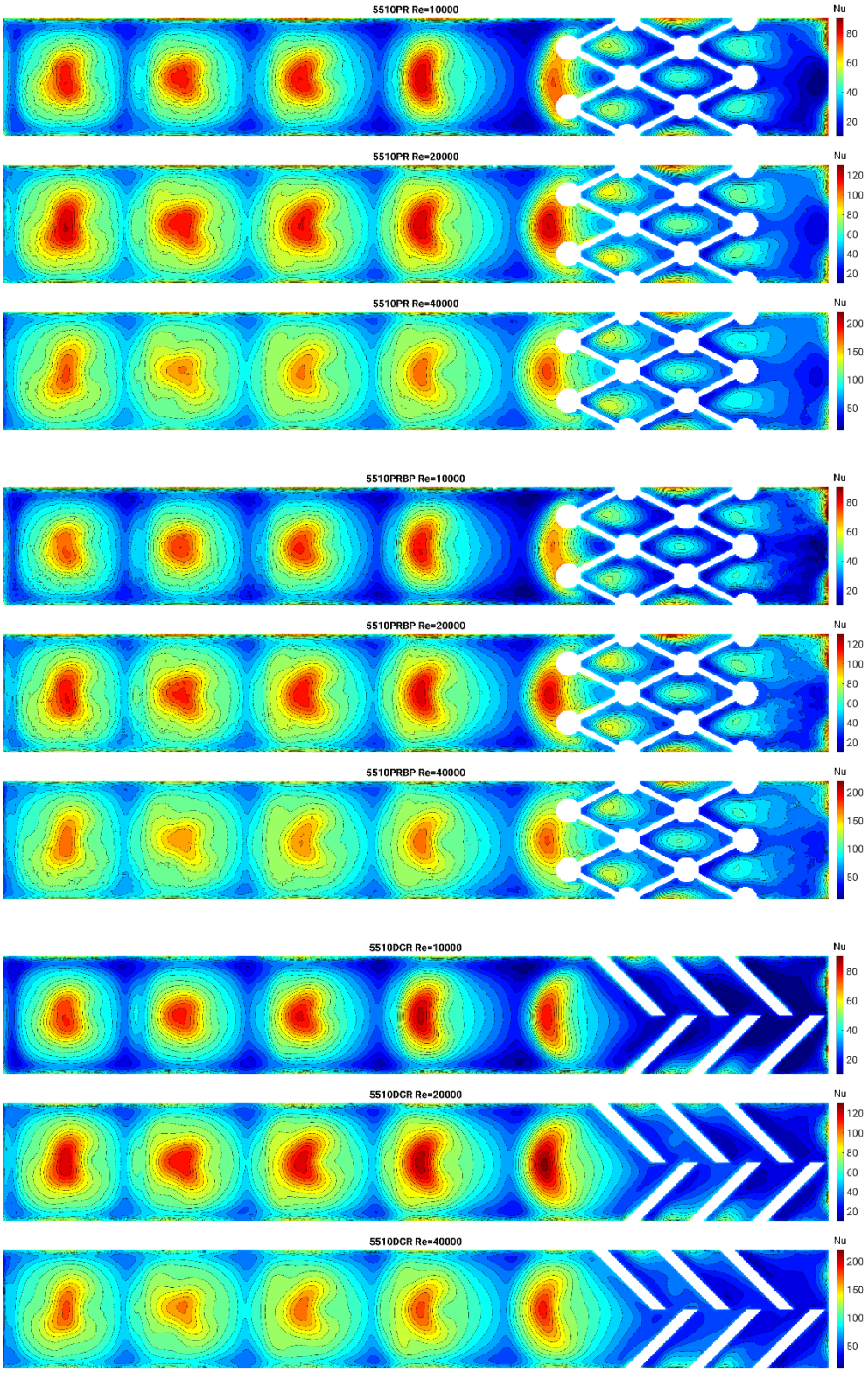
5510PR Re=10000
Nu
80
60
40
20
5510PR Re=20000
Nu
120
100
80
60
40
20
5510PR Re=40000
Nu
200
150
100
50
5510PRBP Re=10000
Nu
80
60
40
20
5510PRBP Re=20000
Nu
120
100
80
60
40
20
5510PRBP Re=40000
Nu
200
150
100
50
5510DCR Re=10000
Nu
80
60
40
20
5510DCR Re=20000
Nu
120
100
80
60
40
20
5510DCR Re=40000
Nu
200
150
100
50

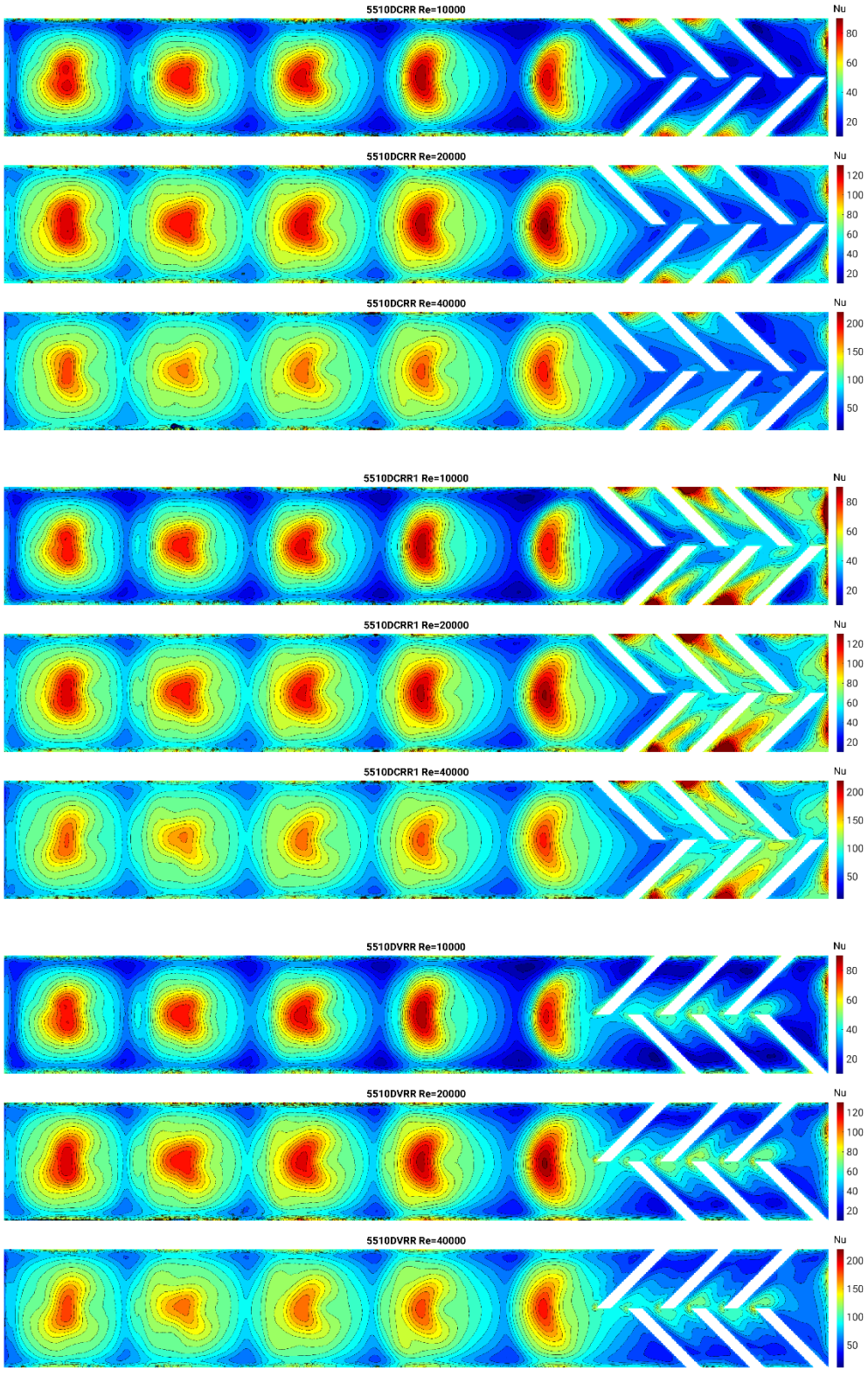
5510DCRR Re=10000
Nu
80
60
40
20
5510DCRR Re=20000
Nu
120
100
80
60
40
20
5510DCRR Re=40000
Nu
200
150
100
50
5510DCRR1 Re=10000
Nu
80
60
40
20
5510DCRR1 Re=20000
Nu
120
100
80
60
40
20
5510DCRR1 Re=40000
Nu
200
150
100
50
5510DVRR Re=10000
Nu
80
60
40
20
5510DVRR Re=20000
Nu
120
100
80
60
40
20
5510DVRR Re=40000
Nu
200
150
100
50

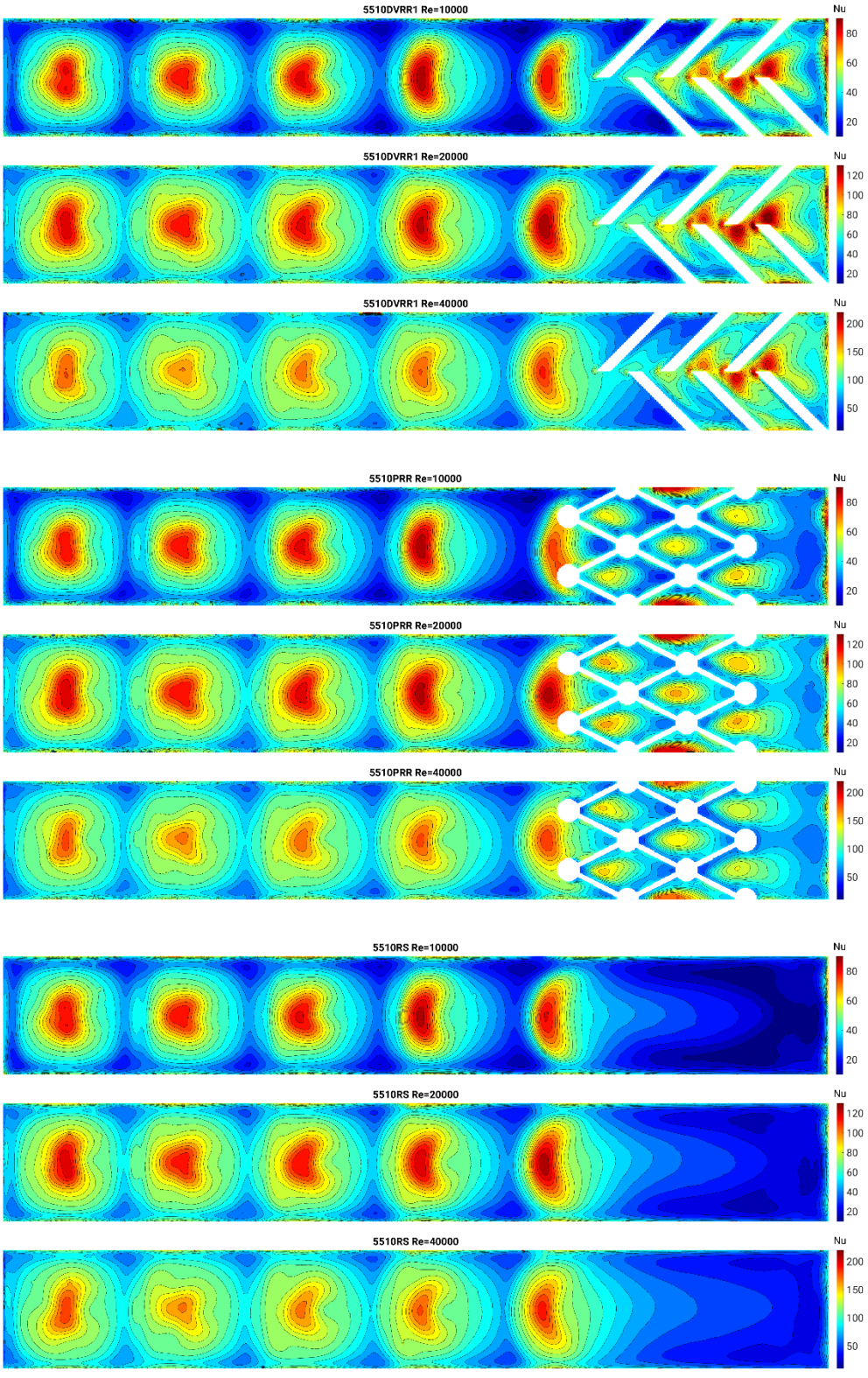
5510DVRR1 Re=10000
Nu
80
60
40
20
5510DVRR1 Re=20000
Nu
120
100
80
60
40
20
5510DVRR1 Re=40000
Nu
200
150
100
50
5510PRR Re=10000
Nu
80
60
40
20
5510PRR Re=20000
Nu
120
100
80
60
40
20
5510PRR Re=40000
Nu
200
150
100
50
5510RS Re=10000
Nu
80
60
40
20
5510RS Re=20000
Nu
120
100
80
60
40
20
5510RS Re=40000
Nu
200
150
100
50